The nucleoid as a scaffold for the assembly of bacterial signaling complexes

Audrey Moine[1], Leon Espinosa[1], Eugenie Martineau[1], Mutum Yaikhomba [2], P J Jazleena[2], Deborah Byrne[3], Emanuele G. Biondi[1], Eugenio Notomista[4], Matteo Brilli[5], Virginie Molle[6], Pananghat Gayathri[2], Tâm Mignot[1*] and Emilia M.F. Mauriello[1*]

[1]Laboratoire de Chimie Bactérienne, CNRS-Université Aix-Marseille, Marseille, France; [2]Biology Division, Indian Institute of Science Education and Research, Pune, India; [3]Protein Purification Platform, Institut de Microbiologie de la Méditerranée, CNRS, Marseille, France; [4]Dipartimento di Biologia, Università degli Studi di Napoli "Federico II", Naples, Italy; [5]Centre for Research and Innovation, Fondazione Edmund MachTrento, Italy; [6]Laboratoire de Dynamique des Interactions Membranaires Normales et Pathologiques, CNRS-Universités de Montpellier II et I, Montpellier, France.

[*]Correspondence to:
Emilia M.F. Mauriello
Laboratoire de Chimie Bactérienne,
CNRS-Université Aix-Marseille
31 Chemin Joseph Aiguier, Marseille 13402, France
Tel. +33491164321
Email : emauriello@imm.cnrs.fr

Tâm Mignot
Laboratoire de Chimie Bactérienne,
CNRS-Université Aix-Marseille
31 Chemin Joseph Aiguier, Marseille 13402, France
Tel. +33491164348
Email: tmignot@imm.cnrs.fr

Running Title: The *Myxococcus xanthus* FrzCD cytoplasmic chemoreceptor binds DNA to enhance the signaling activity of Che-like clusters

ABSTRACT

The FrzCD chemoreceptor from the gliding bacterium *Myxococcus xanthus* forms cytoplasmic clusters that occupy a large central region of the cell body also occupied by the nucleoid. In this work, we show that FrzCD directly binds to the nucleoid with its N-terminal positively charged tail and recruits active signaling complexes at this location. The FrzCD binding to the DNA leads to the formation of multiple distributed clusters that explore constrained areas. This supra-molecular organization is required for cooperative interactions between clustered receptors, in turn important for the modulation of bacterial social behaviors.

INTRODUCTION

The bacterial cytoplasm is not a homogeneous solution of macromolecules, but rather a highly organized and compartmentalized space where the clustering and segregation of macromolecular complexes at certain cell regions confers functional efficiency (Typas and Sourjik, 2015). Bacterial chemoreceptors represent a versatile model system to study the subcellular localization of macromolecules, as they are universally present in prokaryotes where they form highly ordered arrays that occupy different positions in cells. Chemoreceptors, also called Methyl-accepting Chemotaxis Proteins (MCP), are capable of transducing external signals to downstream signaling pathways where phospho-cascades, initiating at the level of histine kinases CheAs and culminating at the level of output response regulators CheYs, translate the initial signal into cell behaviors such as regulation of motility, cell development or aggregation (Sourjik and Berg, 2002; Berleman and Bauer, 2005; Bible *et al.*, 2012). A common feature of the MCPs is their ability to form highly ordered hexagonal structures, which, by cryoelectron tomography, look like lattices with each unit composed of an MCP trimer of dimers, two CheW docking proteins and one CheA dimer (Studdert and Parkinson, 2005; Li *et al.*, 2011; Briegel *et al.*, 2012a; Liu *et al.*, 2012). Receptor clustering is not strictly required for signal transduction, as one functional unit is enough to generate phosphorylated CheY (Francis *et al.*, 2002; Li *et al.*, 2011; Li and Hazelbauer, 2011; Piñas *et al.*, 2016). However, MCP clustering is essential to ensure the amplification of the initial signal, which is a direct consequence of the cooperative interactions between clustered chemoreceptors (Sourjik and Berg, 2004; Ames and Parkinson, 2006; Li and Hazelbauer, 2014; Piñas *et al.*, 2016; Frank *et al.*, 2016).

While the MCP lattices have been described as universal among prokaryotes (Briegel *et al.*, 2015) their subcellular localization and distribution can vary among different bacterial species, often reflecting life style complexity, behaviors and functions. For example,

Escherichia coli MCPs localize in one or two polar clusters and more lateral clusters appear as cells become longer (Thiem and Sourjik, 2008). Differently, the TlpT cytoplasmic chemoreceptor from *Rhodobacter sphaeroides* forms a cluster positioned at the center of cells or two clusters positioned at the two and three cell quarters (Thompson *et al.*, 2006). The determinants of these different localization patterns also vary. In *E. coli*, membrane-anchored MCPs form clusters stochastically and through a self-assembly mechanism (Thiem and Sourjik, 2008). The TlpA *Bacillus subtilis* polar chemoreceptor recognizes and associates with strongly curved membrane regions generated during cell septation. These regions become the new poles after cell division, which explains the TlpA polar localization (Strahl *et al.*, 2015). While in *E. coli* and *B. subtilis* the polar targeting of bacterial chemoreceptors is due to intrinsic properties of these proteins, in *Vibrio* species the Che proteins are recruited to the cell poles by a set of specialized proteins responsible of the general maturation of these cell regions (Ringgaard *et al.*, 2011; Ringgaard *et al.*, 2014). The presence of CheWs and CheAs also seem to be universally important in chemoreceptor cluster formation (Sourjik and Berg, 2000; Martin *et al.*, 2001).

Myxococcus xanthus is a gliding bacterium that uses the Frz chemosensory system to modulate the frequency at which cells periodically reverse the direction of their movement on solid surfaces to reorient in the environment, analogously to controlled tumbles in *E. coli* (Blackhart and Zusman, 1985). The Frz regulation of directionality in *M. xanthus* is essential to achieve fruiting body formation, a behavior that bacteria initiate when they are exposed to unfavorable growth conditions. In the Frz pathway, the FrzCD chemoreceptor activates the autophosphorylation of a CheA-CheY fusion, FrzE, which in turn phosphorylates the response regulator FrzZ (Guzzo *et al.*, 2015). The system also possesses two CheW homologues (FrzA and FrzB), a methyltransferase (FrzF) and methylesterase (FrzG). The chemoreceptor of the Frz pathway, FrzCD, lacks the transmembrane and periplasmic

domains, which are replaced by a N-terminal domain of unknown function (Bustamante *et al.*, 2004). When FrzCD was first localized in cells, it appeared organized in multiple dynamic cytoplasm clusters that aligned when cells made side-to-side contacts, which has been proposed to be part of a signaling process that synchronizes cell reversals (Mauriello, Astling, *et al.*, 2009). However the determinants of FrzCD localization and its exact link with the regulation of the cell reversal are still unclear.

In this work we show that FrzCD forms cytoplasmic signaling clusters by directly binding to the nucleoid. Analogously to membrane chemotaxis clusters in *E. coli*, nucleoid binding and cluster formation confer to the Frz system important regulatory properties such as signal amplification. We propose that the nucleoid functions as a scaffold for the formation of bacterial chemosensory complexes like the membrane for enteric chemosensory systems.

RESULTS

The Frz chemosensory system co-localizes with the nucleoid of different bacterial species

Fluorescence microscopy has shown that a FrzCD-GFP fusion appears as multiple distributed clusters co-localizing with the nucleoid in *M. xanthus* cells (Figure 1A, 1B and Figure 1-figure supplement 1) (Mauriello, Astling, *et al.*, 2009; Moine *et al.*, 2014; Kaimer and Zusman, 2016). It has been also shown that an inducible FrzE-YFP fusion colocalizes with FrzCD at the nucleoid (Kaimer and Zusman, 2016). To further analyze the co-localization of FrzCD and FrzE with the nucleoid, we first constructed a strain expressing a *frzE-mcherry* fusion that replaced the *frzE* locus and is, thus, expressed under its endogenous promoter. The chimeric protein was functional (Figure 1-figure supplement 2) and formed clusters very similar to that of FrzCD and also co-localizing with the *M. xanthus* nucleoid (Figure 1A, 1B and Figure 1-figure supplement 1).

To directly show that the nucleoid supports Frz protein localization, we constructed a *M. xanthus* conditional mutant that lacked ParB, a protein important for nucleoid segregation whose absence causes the presence of anucleated cells, cells with abnormal nucleoid condensation and cells where the division septum is improperly positioned over the nucleoid ("guillotines") (Harms *et al.*, 2013; Iniesta, 2014). When *frzCD-gfp* and *frzE-mCherry* were expressed in the *parB* mutant, we observed that both FrzCD and FrzE clusters always co-localized with the nucleoid and cells lacking the nucleoid also lacked Frz clusters. Similarly, in cells with "guillotines", septa formed in regions occupied by both the nucleoid and Frz clusters instead than in DNA-free regions (Figure 1E).

As a control, we looked at the cellular localization of another chemoreceptor fusion, DifA-GFP, in the absence of *parB*. DifA has been recently shown to form membrane bound and uniformly distributed clusters (Moine *et al.*, 2014). In the absence of *parB*, even cells without nucleoid still carried DifA-GFP clusters and these clusters localized similar to the wild type

(Moine *et al.*, 2014) (Figure 1E). These results confirmed that nucleoid-mediated cluster formation is a specific feature of Frz proteins.

To test if FrzCD and FrzE were capable of associating with the nucleoid independently of each other, we expressed *frzE-mcherry* in a strain lacking *frzCD* and *frzCD-gfp* in a strain lacking *frzE* (Mauriello et al., 2009 and this study). As previously shown, in the absence of FrzCD, FrzE-mCherry was homogeneously dispersed in the cytoplasm, and notably also in the polar regions (Figure 1A, 1B and Figure 1-figure supplement 1) (Mauriello, Astling, *et al.*, 2009; Kaimer and Zusman, 2016). Here we additionally showed that in the absence of *frzE*, FrzCD was no longer capable to form clusters, but the fluorescent signal was still retained towards the center of the cell body and strictly co-localized with the nucleoid (Figure 1A-D and Figure 1-figure supplement 1). The aberrant localization patterns observed in the deletion mutants were not due to a change in protein levels (Figure 1-figure supplement 3). Thus, this result confirms that both FrzCD and FrzE are important for cluster formation, whereas FrzCD is responsible for the recruitment of FrzE to the nucleoid.

To check whether the association between FrzCD and the nucleoid was *M. xanthus*-specific, we constructed an *E. coli* strain expressing *frzCD-gfp* from a plasmid and under the control of an IPTG inducible promoter. Under these conditions, FrzCD also co-localized with the nucleoid and this co-localization was particularly evident in elongated undivided cells containing multiple segregated nucleoids (Figure 2A-D).

These observations suggest that FrzCD can associate with the chromosomes of different bacterial species, either directly or by the aid of a docking factor common to *M. xanthus* and *E. coli*.

FrzCD directly binds to the DNA

The possibility that FrzCD interacted with the nucleoid was puzzling especially considering that the direct binding between a chemoreceptor and the DNA has not been reported prior to this study. To explore this possibility, we generated a 6His-tagged FrzCD version, purified it from *E. coli* and tested its ability to form complexes with DNA. FrzCD binds directly to DNA because its presence altered DNA mobility on agarose gels (Figure 3A). Binding did not require extended DNA fragments because it was also observed with oligomers of DNA as small as 69 bp (Figure 3-figure supplement 1). Moreover, FrzCD DNA-binding did not seem to depend on the DNA sequence nor on its GC content (Figure 3-figure supplement 1) as anticipated by the *in vivo* results showing that FrzCD is distributed all over the nucleoid in the absence of FrzE (Figure 1A and B).

The shift pattern depended on the FrzCD concentration (Figure 3A). More specifically, the shift of DNA fragments gradually increased as the FrzCD concentration was increased (Figure 3A and Figure 3-figure supplement 1). Such migration profiles have been previously described for proteins that can nucleate on DNA molecules in a non -specific manner, i.e. some Type Ib ParA-like proteins (Hester and Lutkenhaus, 2007; Castaing *et al.*, 2008). However, to exclude that such profiles were due to the formation of FrzCD unfolded aggregates, we checked the oligomerization state of our purified 6His-FrzCD. As expected for an MCP, FrzCD forms a homogenous dimer in solution, corresponding to a molecular weight of ~ 90 kDa (Figure 3-figure supplement 1). Last, 6His-FrzCD activated the autophosphorylation of the FrzE kinase *in vitro*, proving that it is functional (Figure 3-figure supplement 1).

While FrzCD does not appear to bind specific DNA motifs in vitro, it could bind to specific sites *in vivo* (perhaps with the help of additional factors), explaining the formation of clusters. To test this possibility, we performed chromatin-immunoprecipitation (ChIP) experiments

using the *frzCD-gfp* strain and polyclonal GFP antibodies. As expected, FrzCD-GFP but not a FrzCD variant that cannot bind DNA (see below) was able to co-immunoprepicipate significant amounts of DNA. Deep-sequence (ChIP-Seq) (Fioravanti *et al.*, 2013) of the immunoprecipitated DNA revealed no enrichment in the pool of DNA fragments obtained with the ChIP meaning that FrzCD-GFP can bind any DNA sequence from the *M. xanthus* genome (Figure 3-figure supplement 2; the ChipSeq results have also been deposited on GEO (https://www.ncbi.nlm.nih.gov/geo/) and an accession number is being created). As a positive control we used a *parB-yfp* strain (Harms *et al.*, 2013). In this case, as expected, the nucleoid region corresponding to positions 9,109 to 9,110 Kb and containing *parS* (Harms *et al.*, 2013) was highly represented in the DNA pool obtained with ParB-YFP (Figure 3-figure supplement 2). We conclude that FrzCD binds DNA in a non sequence-specific manner to recruit FrzE and thus form clusters containing Frz signaling complexes.

The FrzCD N-terminal region is required for the FrzCD DNA binding

Beside a very conserved C-terminal methylation domain, FrzCD contains a unique 137 residue N-terminal region (Figure 3B). We then asked whether this region corresponded to the FrzCD nucleoid-binding domain and tested its ability to form complexes with the DNA in our gel shift assays. Indeed, the FrzCD N-terminal domain (FrzCD$^{\Delta 131\text{-}417}$) also provoked a mobility shift of DNA fragments of different length, albeit at a lower efficiency (compare Figure 3A and C). On the other hand, the FrzCD C-terminal methyl-accepting domain alone (FrzCD$^{\Delta 1-130}$) did not associate with any DNA fragment (Figure 3D) showing that the methylation domain does not bind DNA.

To confirm a direct interaction between FrzCD and DNA and also better compare the DNA-binding properties of FrzCD and FrzCD$^{\Delta 131\text{-}417}$, we performed DNA-protein interaction experiments using Bio-Layer Interferometry (BLI), a technique previously used to study

protein-protein interactions (Arlet *et al.*, 2014). FrzCD and DNA interaction was also detected in this assay (Figure 3E). Consistent with the gel-shift experiments, binding appeared complex and could not be fitted to a 1:1 interaction model, precluding precise determination of a K_D. Nevertheless, when we compared the DNA binding curves of FrzCD$^{\Delta 131\text{-}417}$ and FrzCD, the results confirmed that FrzCD$^{\Delta 131\text{-}417}$ binds the DNA at a lower efficiency than FrzCD (showing slower association and faster dissociation, Figure 3E).

By further analyzing the FrzCD N-terminal domain, we realized that it contains a positively charged peptide of approximately 30 amino acids followed by a more negative region predicted to contain alpha helices (Figure 3B and F, Figure 3-figure supplement 3). By searching for homologs in the UniProtKB/SwissProt Data Base, we found that such FrzCD N-terminal basic peptide was similar to the basic tail present at the N terminus of eukaryotic histones (Figure 3-figure supplement 3) whose deletion has been shown to substantially affect histone-DNA interactions and decrease nucleosome stability (Parra *et al.*, 2006; Iwasaki *et al.*, 2013). To test whether this sequence had a histone-tail-like function in the binding of FrzCD to DNA *in vitro*, we generated a 6His-tagged FrzCD version only lacking the basic amino acid sequence from residue 7 to 27 (FrzCD$^{\Delta 7\text{-}27}$), purified it from *E. coli* and tested its ability to form complexes with the DNA in our gel shift assays. Remarkably, FrzCD$^{\Delta 7\text{-}27}$ did not shift the migration of DNA fragments on agarose gels, similarly to FrzCD$^{\Delta 1\text{-}130}$ missing the entire N-terminal domain (Figure 3D and 3G). In the BLI assay, binding of FrzCD$^{\Delta 7\text{-}27}$ to DNA was still detectable, however it was severely impaired (Figure 3E). This result suggests that the positively charged motif is required for efficient DNA binding but it may not be the sole determinant.

The different DNA binding efficiencies of the four FrzCD, FrzCD$^{\Delta 1-130}$, FrzCD$^{\Delta 131\text{-}417}$ and FrzCD$^{\Delta 7\text{-}27}$ alleles were not due to altered protein stability and folding because all

recombinant proteins, except as expected FrzCD$^{\Delta 131\text{-}417}$ (the signaling domain) were able to activate the autophosphorylation of the FrzE kinase *in vitro* (Figure 3-figure supplement 1).

The binding of FrzCD to the nucleoid is required for FrzCD cluster formation *in vivo*

To check whether the absence of the N terminus or the basic tail also affected the binding of FrzCD to DNA *in vivo*, we used *M. xanthus* strains expressing *frzCD*$^{\Delta 6\text{-}130}$*-gfp* or *frzCD*$^{\Delta 7\text{-}27}$*-gfp* at the *frzCD* locus (Mauriello *et al.*, 2009 and this study). The FrzCD$^{\Delta 6\text{-}130}$-GFP and FrzCD$^{\Delta 7\text{-}27}$-GFP fluorescence appeared mostly diffused, also occupying the polar regions (Figure 1A-D). The two protein fusions could only rarely form short-lived clusters that localized anywhere in the cells (not only at the central region). In all cases, the aberrant localization patterns where not due to protein stability (Figure 1-figure supplement 3). In addition, when FrzCD$^{\Delta 6\text{-}130}$-GFP and FrzCD$^{\Delta 7\text{-}27}$-GFP were produced in *E. coli* they also lost their co-localization with the nucleoid. However, instead of looking dispersed in the cytoplasm as in *M. xanthus*, FrzCD$^{\Delta 6\text{-}130}$-GFP and FrzCD$^{\Delta 7\text{-}27}$-GFP were confined at one cell pole in *E. coli*. It is likely that FrzCD$^{\Delta 6\text{-}130}$-GFP and FrzCD$^{\Delta 7\text{-}27}$-GFP formed aggregates targeted to the poles due to the absence of the nucleoid anchor (Figure 2).

FrzCD cluster dynamics are confined to small nucleoid areas

To understand how FrzCD clusters are formed along the nucleoid, we analyzed the cluster dynamics at high temporal resolution. Contrarily to previous assumptions based on lower resolution analysis (Mauriello, Astling, *et al.*, 2009), this analysis showed that FrzCD clusters are quite fixed and only featured by Brownian-like motions in highly constrained areas of the nucleoid (Figure 4A-C). This mobility decreased with the increase of cluster intensity, suggesting that clusters containing more molecules might be more tightly anchored to the chromosome and, hence, more fixed (Figure 4D). To test whether the signaling state of

FrzCD also affects the cluster mobility, we tested whether clusters were also constrained in strains carrying point mutations either generating FrzCD loss of function or, oppositely, FrzCD gain of function (Astling *et al.*, 2006; Mauriello, Astling, *et al.*, 2009; Guzzo *et al.*, 2015). There were no notable differences between the tested conditions, suggesting that signaling does not affect the nucleoid dynamics of Frz signaling complexes along the nucleoid (Figure 4E).

The nucleoid-dependent assembly could promote cooperative interactions between FrzCD receptors

Consistent with transmembrane chemosensory clusters (Francis *et al.*, 2002; Li *et al.*, 2011; Li and Hazelbauer, 2011; Piñas *et al.*, 2016), the formation of Frz nucleoid-associated clusters is not strictly required for signaling. In fact, it has been previously shown that a *frzCD*$^{\Delta 6\text{-}130}$ strain, where FrzCD molecules can no longer bind DNA and are, thus, diffused (Figure 1), can still produce reversals (Bustamante et al., 2004). This is not surprising because in *E. coli* chemosensory cluster formation is also not critical for the signal transduction, but it confers properties such as the amplification of signal, a direct consequence of the cooperative interactions between clustered chemoreceptors (Sourjik and Berg, 2004; Ames and Parkinson, 2006; Li and Hazelbauer, 2014; Piñas *et al.*, 2016; Frank *et al.*, 2016). Thus, we decided to check if the formation of Frz clusters also led to cooperativity in the signaling activity of the Frz chemosensory system. For this, we took advantage of a newly developed microfluidic single cell assay where the frequency of reversals can be measured as a function of increasing concentrations of an artificial Frz-signal activator, the isoamyl alcohol (IAA) (Guzzo *et al.*, 2015). Consistent with previous observations (Guzzo *et al.*, 2015), in cells where FrzCD formed nucleoid bound clusters, IAA induced a dose-dependent response with a sigmoidal shaped curve that could be fitted by the Hill equation with a coefficient n = 3.017 +/- 0.2 (P =

0.0007), which is significantly higher than one and reveals the presence of cooperativity in the FrzCD activity (Figure 5A). Such response is FrzCD-dependent because a *ΔfrzCD* strain does not reverse at any IAA dose (Figure 5A). In the *frzCD*$^{\Delta 6\text{-}130}$ mutant, the dose-dependent response curve to IAA resulted to a Hill coefficient n = 1.15 +/- 0.01 (P = 0.008) when it was fitted by the Hill equation, revealing that cooperation is lost in this mutant. These results suggest that while the IAA response in the *frzCD*$^{\Delta 6\text{-}130}$ mutant only depends on the number of the FrzCD$^{\Delta 6\text{-}130}$ molecules in the cytoplasm, in cells where FrzCD formed nucleoid bound clusters, such response also depends on the supra-molecular organization of the FrzCD proteins, presumably because of cooperative protein interactions in the clusters (Lai *et al.*, 2005; Li and Hazelbauer, 2014; Piñas *et al.*, 2016). This signal amplification is advantageous to *M. xanthus* social behaviors because swarming and predation are defective in the *frzCD*$^{\Delta 6\text{-}130}$ mutant compared to the wild type (Figure 5B and C).

DISCUSSION

In this work, we show that analogously to how transmembrane chemoreceptors use the bacterial inner membrane as a platform to form the well described arrays of trimers of dimers (Briegel *et al.*, 2012b), the *M. xanthus* Frz system forms signaling clusters on the bacterial chromosome. Cluster assembly is directed by the chemoreceptor FrzCD, which binds to the DNA by a N-terminal domain carrying a positively charged tail similar to that found in eukaryotic histones (Parra *et al.*, 2006; Iwasaki *et al.*, 2013). While the binding of FrzCD to DNA is essential to target the Frz chemosensory system to the nucleoid, it is not sufficient for Frz cluster formation, as it requires downstream interactions with the FrzE kinase. Because FrzCD appears to bind DNA in a non-sequence specific manner, DNA-bound clusters do not occupy fixed localization sites and move across small areas on the nucleoid surface. Analogous to trans-membrane proteins diffusing in the bacterial membrane, the FrzCD cluster dynamic behavior may be affected by the size of the complex (and thus the number of interactions with DNA), explaining why bright clusters show Brownian-like motions that only explore constrained nucleoid areas.

Several lines of evidence suggest that the Frz cluster formation on the nucleoid occurs in a stochastic manner similarly to the assembly of the *E. coli* Che lattices in the membrane. First, the initial binding of FrzCD to DNA might take place anywhere on the nucleoid as such binding is not DNA-sequence specific. Once recruited to the nucleoid, small FrzCD foci diffuse, non-directionally, across confined small areas until they might nucleate large fixed clusters by attracting more FrzCD molecules. “Newborn” FrzCD foci might also, at one point, be incorporated by existing neighboring clusters. Thus, the areas explored by FrzCD clusters might represent the minimal critical distance from other clusters at which foci can exist. The existence of such minimal critical distance is supported by the fact that the number of Frz clusters increases linearly with the nucleoid size (Figure 1-figure supplement 4), suggesting

that more clusters can form when more surface becomes available. Thus, like for transmembrane chemoreceptors, FrzCD molecules might either nucleate new dynamic foci if they are far enough from existing clusters, or encounter and join neighboring clusters.

Transmembrane chemoreceptors are arrayed in a monolayer tightly associated with the inner membrane (Briegel *et al.*, 2009). However, in the absence of a scaffold *Vibrio sp.* and *R. sphaeroides* cytoplasmic chemosensory arrays, are instead organized in two sandwiched arrays (Briegel *et al.*, 2014; Briegel *et al.*, 2015; Briegel *et al.*, 2016). Our data suggest that the *M. xanthus* chromosome functions as a platform to form signaling clusters, much like the inner membrane supports transmembrane chemosensory complexes. In the future, it will be interesting to test if the Frz proteins, indeed, form single layered arrays at the surface of the chromosome by Cryo-EM tomography.

But, what is the outcome of this nucleoid driven cluster assembly? FrzCD cluster formation has been previously been associated to regulation of the cell reversal frequency in response to cell-cell contact. In fact, FrzCD clusters align in adjacent *M. xanthus* cells, a behavior that also seemed to induce cell reversals (Mauriello, Astling, *et al.*, 2009). The authors' argument in favor of a retro-regulated FrzCD cluster rearrangement in response to cell contact was that adjacent cells of a *frzE* strain, which also seemed to form FrzCD-GFP clusters even if more diffused, did not produce cluster alignment. In light of our new results, what seemed to be more diffused FrzCD clusters in the *frzE* strain, are, in fact, FrzCD molecules dispersed on the nucleoid. Moreover, we now show that the Frz cluster organization is independent on the Frz signaling activity. Thus, the observed FrzCD cluster alignment might be more likely determined by similar dynamic rearrangements of the nucleoid of adjacent cells rather than by an active regulated mechanism.

Therefore, a simpler outcome of the nucleoid-driven Frz cluster assembly could be to confer to a cytoplasmic receptor the universal properties of transmembrane receptors but here, in

response to intracellular signals. One of these properties is the signal amplification, which, in enteric bacteria, strictly requires the MCP clustering to the membrane. Remarkably, this work as well as previous studies shows that wild type *M. xanthus* cells respond to increasing concentrations of the Frz activator IAA with a dose-dependent response curve typical of a cooperative response that strongly suggests the presence of signal amplification. Analogously to enteric bacteria, signal amplification must be due to the supra-molecular organization of FrzCD receptors on the nucleoid, because such property is lost in FrzCD$^{\Delta 6\text{-}130}$ lacking the nucleoid binding domain. In cells of this strain, the reversal frequencies increase linearly with the IAA doses, suggesting that, in this case, signaling is only function of the number of activated receptor-signaling complexes dispersed in the cytoplasm.

Why does FrzCD need to form many and not just one single cluster? One possibility could be to prevent the diffusion of CheY-P to be a limiting factor in the control of the polar and lateral motility motors due to the length of *M. xanthus* cells (5-10 μm in average). However, a more attractive explanation could be that the nucleoid-dependent formation of multiple distributed clusters represents a simple mechanism to segregate clusters during cell division without the need for a faithful partitioning system (Figure 1-figure supplement 5). Such partitioning system would be, in fact, likely required in the presence of a single cluster like in *R. sphaeroides* where PpfA ensures the faithful segregation of Tlp clusters (Thompson *et al.*, 2006; Ringgaard *et al.*, 2011).

Finally, the analysis of the FrzCD sequences from some related species of δ-proteobacteria shows that while the FrzCD C-terminal region is very conserved, its N-terminus largely varies. Nevertheless, the FrzCD N-terminus always shows a positively charged sequence (Figure 3-figure supplement 4) suggesting that the non sequence-specific recruitment of Frz

proteins to the nucleoid essentially requires the presence of a positively charged protein domain rather than a specific amino acid sequence.

This type of cellular organization may be common to other bacterial macromolecular complexes to provide important regulatory functions. In this sense, the Frz example provides new perspectives to the role of the bacterial nucleoid as a scaffold for the spatial control of cellular functions.

MATERIALS AND METHODS

Bacterial strains, plasmids and growth

Strains and plasmids are listed in Table S1 and S2. *M. xanthus* strains were grown at 32°C in CYE rich media as previously described. *Pcuo::parB-ΔparB* cells were grown at 32°C in CTT supplied with 300 µM $CuSO_4$.

Plasmids were introduced into *M. xanthus* cells by electroporation. Deletions and GFP fusions were inserted in frame to avoid polar effects on the downstream gene expression. These strains were obtained by homologous recombination based on a previously reported method using the pBJ113 or pBJ114 vectors (Bustamante *et al.*, 2004; Moine *et al.*, 2014). To generate strains expressing GFP or mCherry fusion proteins, we constructed DNA cassettes including the last approximately 800 bp of each gene, with the exception of the stop codon; the gene encoding the *egfp* or *mcherry* genes from pEGFP-N1 (Invitrogen) or pEM147 (Mauriello, Nan, *et al.*, 2009) excluding the start codon and including the stop codon; the intergenic region between the gene of interest and its immediately downstream gene, if any; the first 800 bp of the downstream gene.

To construct the *parB* conditional mutant, we transferred the previously described *parB* conditional depletion (Harms *et al.*, 2013) in our wild type strain, DZ2 (Harms *et al.*, 2013; Iniesta, 2014).

To construct strains carrying a FrzS-YFP fusion, we used the pEFrzSY plasmid (Guzzo *et al.*, 2015)

Escherichia coli cells were grown under standard laboratory conditions in Luria-Bertani broth supplemented with antibiotics if necessary.

For swarming assays, cells (5 µl) at a concentration of 5×10^9 cfu ml^{-1} were spotted on CYE agar plates and incubated at 32°C and photographed after respectively 48h with an Olympus SZ61 binocular stereoscope. For predation assays, *E. coli* (3µl at a concentration of 5×10^9 cfu

ml^{-1}) and *M. xanthus* cells (3µl at a concentration of 5×10^9 cfu ml^{-1}) were spotted at 0.7 mm distance from each other on CF agar plates, incubated at 32°C and photographed after 72 h.

Protein purification

BL21(DE3) [F$^-$ ompT hsdSB(rB$^-$ mB$^-$) gal dcm (DE3)] cells were grown in Luria-Bertani broth supplemented 100 µg/ml ampicillin to mid-exponential phase at 37°C. For the experiments shown on Figure 3 and phosphorylation assays on Figure 3-figure supplement 1, overexpression was induced by adding 0,1 mM IPTG for cells containing plasmid pEM414 or 0,5mM for pEM415 and pEM433. Cells were then grown at 16°C over night. Cells were washed and resuspended in lysis buffer (50 mM TrisHCl, pH 8; 300 mM NaCl; 100 µg/ml PMSF; 30 U/mL Benzonase) and lysed at the French press. The cell lysates were centrifuged at 4°C for 30 min at 13000× rpm. Soluble tagged His_6-proteins were purified on 1ml HisTrap^{TM}FF columns (GE Healthcare) and desalted with PD-10 columns (GE Healthcare). Ultimately, purified proteins were eluted in 50 mM TrisHCl, pH 8 and 300 mM NaCl.

For the experiments shown on Figure 3-figure supplement 1A-E, the C-terminal-tagged FrzCD-$(His)_6$ was expressed in *E. coli* BL21-AI (Invitrogen) cells. The cells were grown in Luria-Bertani broth containing 100 µg/ml ampicillin at 37°C till OD_{600} of 0.8 – 1.0, and incubated at 30°C for 5 hours post induction. The harvested cells were resuspended in Buffer A (50 mM Tris, 200 mM NaCl, pH 8.0) containing 10 % glycerol and lysed by sonication (Sonics VibraCell, 5 minutes, 60% amplitude, 1" ON, 3" OFF cycle). The cell lysate was spun at 39, 191 g for an hour and the supernatant loaded to a 5-ml HisTrap^{TM} FF (GE Healthcare) equilibrated with Buffer A. Following wash and elution with increasing concentrations (5%, 10%, 20%, 50% and 100%) of Buffer B (50 mM Tris, 200 mM NaCl, 500 mM imidazole, pH 8.0), pure fractions containing FrzCD-H_6 were pooled and dialysed into buffer containing 50 mM Tris, 25 mM NaCl, 1 mM EDTA, pH 8.0 to enable further

purification through ion exchange chromatography using a MonoQ-PE (GE Healthcare) column. The fractions containing the protein were pooled and concentrated using centricons. The protein was finally in buffer containing 50 mM NaCl, 1 mM EDTA and 50 mM Tris pH 8.0 either through dialysis or by buffer exchange during the concentration step. The concentrated protein was flash frozen and stored in small aliquots in -80°C till further use.

Electrophoretic mobility shift assays (EMSA)

EMSAs on Figure 3 were carried out by incubating different concentrations of purified proteins with 10 nM PCR-amplification products of different sizes (Table S4), in buffer (10 mM of TrisHCl at pH 8; 60 mM of NaCl; 10% glycerol). Reactions were incubated for 40 min at 4°C before being loaded on 1% agarose gels. Gel migration was performed in 1X TBE at 4°C for 55 min. Gels were, then, stained with ethidium bromide and revealed at the UV light.

EMSAs for shorter oligos (Figure 3-figure supplement 1 and Table S4) were carried out in buffer containing 50 mM Tris, 50 mM NaCl, 1 mM dithiothreitol and 10 % glycerol, pH 7.4. All the oligonucleotide fragments were PCR-amplification products, except the 69 bp DNA that was generated by annealing the custom-synthesized oligonucleotides (Sigma) corresponding to the 5' to 3' sequence and its complementary strand (Table S4). The samples were incubated at 25°C for 20 min and loaded onto the appropriate % of agarose gel (1% for 1.3 kbp, and electrophoresed for 60 – 90 minutes in 1x TAE (40 mM Tris-Acetate and 1 mM EDTA).

Oligomerization study using Size Exclusion Chromatography coupled with Multi-Angle light Scattering (SEC-MALS)

The expected elongated structure of an MCP precludes estimation of the oligomeric status by size exclusion chromatography alone, and hence we carried out SEC coupled with multi-angle light scattering to estimate the molecular mass in solution. The mass was determined using a Wyatt Dawn Heleos II equipped with light scattering detectors at 18 angles and an Optilab TrEX differential refractive index detector. Protein sample (100 µl of 2 mg/ml solution or 45 µM) was injected into the size exclusion column (BioRad EnRich650) equilibrated with the buffer 50 mM Tris, 50 mM NaCl, pH 8.0, and the run carried out at a flow rate of 0.4 ml/min. The observed molecular masses at various points along the peak in the elution curve were calculated using the protein concentration estimated from the differential refractive index (dRI), and measured scattered intensities. The Debye model in the ASTRA software provided with the equipment was used for fitting the data.

Biolayer interferometry

Protein-DNA interaction experiments were conducted at 25°C with the BLItz instrument from ForteBio (Menlo Park, CA, USA). The BLI consists in a real time optical biosensing technique exploits the interference pattern of white light reflected from two surfaces to measure biomolecular interactions (Concepcion *et al.*, 2009). Purified 6His-FrzCD, 6His-FrzCD$^{\Delta 131\text{-}417}$, 6His-FrzCD$^{\Delta 6\text{-}130}$ and 6His-FrzCD$^{\Delta 7\text{-}27}$ protein ligands were immobilized onto two different Ni-NTA biosensors (ForteBio) in duplicate at 1µM concentrations. A PCR amplified DNA fragment (474bp) with primers AGACCCCCGCACCCACGGAG and TCACGCGGGCTCCGGCTC (Eurogentec) was used as the analyte throughout the study at the 38nM. The assay was conducted in PBS pH 7.5, 0.001% tween-20. The binding reactions were performed with an initial baseline during 30 seconds, an association step at 120 seconds and a dissociation step of 120 seconds with lateral shaking at 2200rpm. A double reference

subtraction (sensor reference and 6His-FrzCD$^{\Delta 1\text{-}130}$) was applied to account for non-specific binding, background, and signal drift to minimize sensor variability.

Chromatin Immunoprecipitation-deep sequencing (ChIp-seq)

ChIp-seq was performed as previously described (Fioravanti *et al.*, 2013). In particular, mid-log phase cells (80 ml, OD_{600} of 0.6) were cross-linked in 10 mM sodium phosphate (pH 7.6) and 1% formaldehyde at room temperature for 10 min and on ice for 30 min thereafter, washed thrice in phosphate buffered saline (PBS) and lysed with lysozyme 2.2 mg ml^{-1} in TES (Tris-HCl 10 mM pH 7.5, EDTA 1 mM, NaCl 100 mM). Lysates (Final volume 1ml) were sonicated (Branson Digital Sonicator 450, Branson Sonic Power. Co., www.bransonic.com/) on ice using 10 bursts of 30 sec (50% duty) at 30% amplitude to shear DNA fragments to an average length of 0.3–0.5 kbp and cleared by centrifugation at 14,000 rpm for 2 min at 4°C. Lysates were normalized by protein content by measuring the absorbance at 280 nm; ca. 7.5 mg of protein was diluted in 1 mL of ChIP buffer (0.01% SDS, 1.1% Triton X-100, 1.2 mM EDTA, 16.7 mM Tris-HCl [pH 8.1], 167 mM NaCl plus protease inhibitors (Euromedex, https://www.euromedex.com/) and pre-cleared with 80 µL of protein-A agarose (Sigma-Aldrich, www.sigmaaldrich.com) and 100 µg BSA. Polyclonal GFP antibodies were added to the remains of the supernatant (1:1,000 dilution), incubated overnight at 4°C with 80 µL of protein-A agarose beads pre-saturated with BSA, washed once with low salt buffer (0.1% SDS, 1% Triton X-100, 2 mM EDTA, 20 mM Tris-HCl (pH 8.1), 150 mM NaCl), high salt buffer (0.1% SDS, 1% Triton X-100, 2 mM EDTA, 20 mM Tris-HCl (pH 8.1), 500 mM NaCl) and LiCl buffer (0.25 M LiCl, 1% NP-40, 1% sodium deoxycholate, 1 mM EDTA, 10 mM Tris-HCl (pH 8.1) and twice with TE buffer (10 mM Tris-HCl (pH 8.1) and 1 mM EDTA). The protein-DNA complexes were eluted in 500 µL freshly prepared elution buffer (1% SDS, 0.1 M NaHCO3), supplemented with NaCl to a final

concentration of 300 mM and incubated overnight at 65°C to reverse the crosslinks. The samples were treated with 2 µg of Proteinase K for 2 h at 45°C in 40 mM EDTA and 40 mM Tris-HCl (pH 6.5). DNA was extracted using QIAgen minelute kit and resuspended in 30 µl of Elution Buffer. ChIp DNA sequencing was performed using Illumina MiSeq and analyzed using Galaxy Web Portal (usegalaxy.org/). Reads were analyzed by MatLab.

Protein sequence analyses

In order to search for homologs of the FrzCD N-terminal domain, the first 130 aminoacids of the FrzCD sequence were BLAST into the UniProtKB/SwissProt Data Base (http://blast.ncbi.nlm.nih.gov). Predictions of secondary structures and protein sequence alignments were obtained with Jpred (Cole *et al.*, 2008) and Clustal Omega (Sievers and Higgins, 2002), respectively. To analyze the FrzCD N-terminal region protein charge, "Sliding window" analyses were performed with Microsoft Excel.

***In vitro* autophosphorylation assay**

In vitro phosphorylation assays were performed with *E. coli* purified recombinant proteins. 4 µg of $FrzE^{kinase}$ were incubated with 1µg of FrzA and increasing concentrations (3µg) of different FrzCD proteins (entire FrzCD, $FrzCD^{c}$, FrzCDΔ6-130, FrzCDΔ7-27 or FrzCDΔ131-417) in 25 µl of buffer P (50 mM Tris-HCl, pH 7.5; 1 mM DTT; 5 mM $MgCl_2$; 50mM KCl; 5 mM EDTA; 50µM ATP, 10% glycerol) supplemented with 200 µCi ml^{-1} (65 nM) of [γ-33P]ATP (PerkinElmer, 3000 Ci $mmol^{-1}$) for 10 minutes at room temperature in order to obtain the optimal $FrzE^{kinase}$ autophosphorylation activity. Each reaction mixture was stopped by addition of 5 × Laemmli and quickly loaded onto SDS-PAGE gel. After electrophoresis, proteins were revealed using Coomassie Brilliant Blue before gel drying. Radioactive proteins were visualized by autoradiography using direct exposure to film (Carestream).

Fluorescence microscopy and image analysis

For fluorescence microscopy analyses, 5 µl of cells from 4 x 10^8 cfu ml^{-1} vegetative CYE cultures were spotted on a thin fresh TPM agar pad at the top a slide (Mignot *et al.*, 2005). A cover slip was added immediately on the top of the pad, and the obtained slide was analyzed by microscopy using a Nikon Eclipse TE2000 E PFS inverted epifluorescence microscope (100 x oil objective NA 1.3 Phase Contrast) (Ducret *et al.*, 2009).

To study the colocalization with the DNA, the TPM agar pads were supplied with 1µg/ml DAPI stain and 1 mM IPTG. Prior to imaging, *E. coli* cells were grown in 1 mM IPTG for one hour then spotted on agar pads containing or not 10µg/ml cephalexin and incubated for 1 hour. Cell fluorescence profiles were obtained with the "plot profile" function of FIJI (Schindelin *et al.*, 2012). FrzCD clusters numbers and distances, nucleoid areas and cell areas were automatically determined and verified manually with the "MicrobeJ" Fiji/ImageJ plugin created by A. Ducret, Brun Lab (http://www.indiana.edu/~microbej/index.html). All data plots and statistical tests were obtained with the R software (https://www.r-project.org/).

To study the dynamic of FrzCD-GFP clusters we automatically tracked clusters (imaged every second) by MicrobeJ and recorded parameters such as the mean square displacement (MSD), the confinement radius and the fluorescence intensity along the time.

For manual image analysis we chose a sample size that allowed an error on the mean (sem) lower than 10%. For results generated by automated analyses, we analyzed all the available samples. We chose all cells where clusters and nucleoids were tractable by our image analysis tools (Fiji and MicrobeJ). For the cluster dynamic determinations we analyzed all clusters that were tractable for at least 5 consecutive frames.

Reversal frequencies

These assays were performed as previously described (Guzzo *et al.*, 2015) by using homemade PDMS glass microfluidic chambers (Ducret *et al.*, 2013) treated with 0.015% carboxymethylcellulose after extensive washing of the glass slide with water. For each experiment, 1mL of a CYE grown culture of OD = 0.5 was injected directly into the chamber and the cells were allowed to settle for 5 min. Motility was assayed after the chamber was washed with TPM 1mM CaCl buffer. For IAA injections, IAA solutions made in TPM 1mM CaCl buffer at appropriate concentrations were injected directly into the channels and motility was assayed directly under the microscope. Time-lapse movies of strains carrying a FrzS-YFP fusion were shot for 20 minutes with frames captured every 15 seconds.

To discriminate bona fide reversal events from stick-slip motions (Guzzo *et al.*, 2015), the fluorescence intensity of FrzS-YFP was measured at cell poles over time. In fact, this protein has been shown to switch from the leading cell pole to the lagging pole when *M. xanthus* cells reverse their movement direction (Mignot *et al.*, 2005). For each cell that was tracked, the fluorescence intensity and reversal profiles were correlated to distinguish bona fide reversals from stick-slip events. About one hundred cells for the wild type and *frzCD*$^{\Delta 1\text{-}130}$ strains and fifty for the *ΔfrzCD* strain were analyzed (refer to Supplementary Table 3 for the exact number of cells analyzed for each strain and IAA dose). The number of reversals was plotted against time. The best fits for the reversal frequencies values at the different IAA doses were obtained with the following Hill equation:

$$\frac{N_{rev}}{\Delta T} = \frac{[IAA]^n}{K_d + [IAA]^n} B + A$$

where the $N_{rev}/\Delta T$ is the number of reversal events per hour; K_d is the apparent affinity constant; *[IAA]* is the IAA dose; *B* is the plateau; *A* is the basal reversal frequency and *n* is the Hill coefficient describing cooperativity. Reversal frequency values for each IAA dose and each strain are the results of two independent biological triplicates.

We chose a sample size that allowed an error on the mean (sem) lower than 10%. We used all cells that moved, remained isolated for at least 20 consecutive frames and where FrzS-YFP foci were detectable by FIJI.

Acknowledgments

We would like to thank Dr. Romain Mercier and Dr. Thierry Doan for their critical reading of the manuscript and discussions; Dr. Mireille Ansaldi for her advise on the EMSA assays; Hanna Bismuth for helping with the ChIP experiments; Pravin Dewangan and Dr. Radha Chauhan for use of the SEC-MALS facility at National Centre for Cell Science, Pune, India.

Research on chemotaxis in our laboratory is funded by the Agence National de la Recherche Jeune Chercheur-Jeune Chercheuse (ANR-14-CE11-0023-01) to E.M.M and the "Fondation Amidex" award to EM and TM. YM, PJJ and PG acknowledge fellowships from INSPIRE, Department of Science and Technology (DST), Govt. of India and the work in the lab at IISER Pune is supported by Innovative Young Biotechnologist Award (IYBA from Department of Biotechnology, Govt. of India), Indian National Science Academy (INSA), and Science and Engineering Research Board (SERB), DST.

BIBLIOGRAPHY

Ames, P., and Parkinson, J.S. (2006) Conformational suppression of inter-receptor signaling defects. *Proc Natl Acad Sci U S A* **103**: 9292–9297.

Arlet, J.-B., Ribeil, J.-A., Guillem, F., Negre, O., Hazoume, A., Marcion, G., *et al.* (2014) HSP70 sequestration by free α-globin promotes ineffective erythropoiesis in β-thalassaemia. *Nature* **514**: 242–246.

Astling, D.P., Lee, J.Y., and Zusman, D.R. (2006) Differential effects of chemoreceptor methylation-domain mutations on swarming and development in the social bacterium Myxococcus xanthus. *Mol Microbiol* **59**: 45–55.

Berleman, J.E., and Bauer, C.E. (2005) Involvement of a Che-like signal transduction cascade in regulating cyst cell development in Rhodospirillum centenum. *Mol Microbiol* **56**: 1457–1466.

Bible, A., Russell, M.H., and Alexandre, G. (2012) The Azospirillum brasilense Che1 chemotaxis pathway controls swimming velocity, which affects transient cell-to-cell clumping. *J Bacteriol* **194**: 3343–3355.

Blackhart, B.D., and Zusman, D.R. (1985) "Frizzy" genes of Myxococcus xanthus are involved in control of frequency of reversal of gliding motility. *Proc Natl Acad Sci U S A* **82**: 8767–8770.

Briegel, A., Ladinsky, M.S., Oikonomou, C., Jones, C.W., Harris, M.J., Fowler, D.J., *et al.* (2014) Structure of bacterial cytoplasmic chemoreceptor arrays and implications for chemotactic signaling. *eLife* **3**: e02151.

Briegel, A., Li, X., Bilwes, A.M., Hughes, K.T., Jensen, G.J., and Crane, B.R. (2012a) Bacterial chemoreceptor arrays are hexagonally packed trimers of receptor dimers networked by rings of kinase and coupling proteins. *Proc Natl Acad Sci U S A* **109**: 3766–3771.

Briegel, A., Li, X., Bilwes, A.M., Hughes, K.T., Jensen, G.J., and Crane, B.R. (2012b) Bacterial chemoreceptor arrays are hexagonally packed trimers of receptor dimers networked by rings of kinase and coupling proteins. *Proc Natl Acad Sci U S A* **109**: 3766–3771.

Briegel, A., Ortega, D.R., Huang, A.N., Oikonomou, C.M., Gunsalus, R.P., and Jensen, G.J. (2015) Structural conservation of chemotaxis machinery across Archaea and Bacteria. *Environ Microbiol Rep* **7**: 414–419.

Briegel, A., Ortega, D.R., Mann, P., Kjær, A., Ringgaard, S., and Jensen, G.J. (2016) Chemotaxis cluster 1 proteins form cytoplasmic arrays in Vibrio cholerae and are stabilized by a double signaling domain receptor DosM. *Proc Natl Acad Sci U S A* **113**: 10412–10417.

Briegel, A., Ortega, D.R., Tocheva, E.I., Wuichet, K., Li, Z., Chen, S., *et al.* (2009) Universal architecture of bacterial chemoreceptor arrays. *Proc Natl Acad Sci U S A* **106**: 17181–17186.

Bustamante, V.H., Martinez-Flores, I., Vlamakis, H.C., and Zusman, D.R. (2004) Analysis of the Frz signal transduction system of Myxococcus xanthus shows the importance of the conserved C-terminal region of the cytoplasmic chemoreceptor FrzCD in sensing signals. *Mol Microbiol* **53**: 1501–13.

Castaing, J.-P., Bouet, J.-Y., and Lane, D. (2008) F plasmid partition depends on interaction of SopA with non-specific DNA. *Mol Microbiol* **70**: 1000–1011.

Cole, C., Barber, J.D., and Barton, G.J. (2008) The Jpred 3 secondary structure prediction server. *Nucleic Acids Res* **36**: W197–W201.

Concepcion, J., Witte, K., Wartchow, C., Choo, S., Yao, D., Persson, H., *et al.* (2009) Label-free detection of biomolecular interactions using BioLayer interferometry for kinetic characterization. *Comb Chem High Throughput Screen* **12**: 791–800.

Ducret, A., Maisonneuve, E., Notareschi, P., Grossi, A., Mignot, T., and Dukan, S. (2009) A microscope automated fluidic system to study bacterial processes in real time. *PloS One* **4**: e7282.

Ducret, A., Théodoly, O., and Mignot, T. (2013) Single cell microfluidic studies of bacterial

motility. *Methods Mol Biol Clifton NJ* **966**: 97–107.
Fioravanti, A., Fumeaux, C., Mohapatra, S.S., Bompard, C., Brilli, M., Frandi, A., *et al.* (2013) DNA Binding of the Cell Cycle Transcriptional Regulator GcrA Depends on N6-Adenosine Methylation in Caulobacter crescentus and Other Alphaproteobacteria. *PLOS Genet* **9**: e1003541.
Francis, N.R., Levit, M.N., Shaikh, T.R., Melanson, L.A., Stock, J.B., and DeRosier, D.J. (2002) Subunit organization in a soluble complex of tar, CheW, and CheA by electron microscopy. *J Biol Chem* **277**: 36755–36759.
Frank, V., Piñas, G.E., Cohen, H., Parkinson, J.S., and Vaknin, A. (2016) Networked Chemoreceptors Benefit Bacterial Chemotaxis Performance. *mBio* **7**.
Guzzo, M., Agrebi, R., Espinosa, L., Baronian, G., Molle, V., Mauriello, E.M.F., *et al.* (2015) Evolution and Design Governing Signal Precision and Amplification in a Bacterial Chemosensory Pathway. *PLoS Genet* **11**: e1005460.
Harms, A., Treuner-Lange, A., Schumacher, D., and Søgaard-Andersen, L. (2013) Tracking of chromosome and replisome dynamics in Myxococcus xanthus reveals a novel chromosome arrangement. *PLoS Genet* **9**: e1003802.
Hester, C.M., and Lutkenhaus, J. (2007) Soj (ParA) DNA binding is mediated by conserved arginines and is essential for plasmid segregation. *Proc Natl Acad Sci U S A* **104**: 20326–20331.
Iniesta, A.A. (2014) ParABS system in chromosome partitioning in the bacterium Myxococcus xanthus. *PloS One* **9**: e86897.
Iwasaki, W., Miya, Y., Horikoshi, N., Osakabe, A., Taguchi, H., Tachiwana, H., *et al.* (2013) Contribution of histone N-terminal tails to the structure and stability of nucleosomes. *FEBS Open Bio* **3**: 363–369.
Kaimer, C., and Zusman, D.R. (2016) Regulation of cell reversal frequency in Myxococcus xanthus requires the balanced activity of CheY-like domains in FrzE and FrzZ. *Mol Microbiol* **100**: 379–395.
Lai, R.-Z., Manson, J.M.B., Bormans, A.F., Draheim, R.R., Nguyen, N.T., and Manson, M.D. (2005) Cooperative signaling among bacterial chemoreceptors. *Biochemistry (Mosc)* **44**: 14298–14307.
Li, M., and Hazelbauer, G.L. (2011) Core unit of chemotaxis signaling complexes. *Proc Natl Acad Sci U S A* **108**: 9390–9395.
Li, M., and Hazelbauer, G.L. (2014) Selective allosteric coupling in core chemotaxis signaling complexes. *Proc Natl Acad Sci U S A* **111**: 15940–15945.
Li, M., Khursigara, C.M., Subramaniam, S., and Hazelbauer, G.L. (2011) Chemotaxis kinase CheA is activated by three neighbouring chemoreceptor dimers as effectively as by receptor clusters. *Mol Microbiol* **79**: 677–685.
Liu, J., Hu, B., Morado, D.R., Jani, S., Manson, M.D., and Margolin, W. (2012) Molecular architecture of chemoreceptor arrays revealed by cryoelectron tomography of Escherichia coli minicells. *Proc Natl Acad Sci U S A* **109**: E1481-1488.
Martin, A.C., Wadhams, G.H., and Armitage, J.P. (2001) The roles of the multiple CheW and CheA homologues in chemotaxis and in chemoreceptor localization in Rhodobacter sphaeroides. *Mol Microbiol* **40**: 1261–1272.
Mauriello, E.M.F., Astling, D.P., Sliusarenko, O., and Zusman, D.R. (2009) Localization of a bacterial cytoplasmic receptor is dynamic and changes with cell-cell contacts. *Proc Natl Acad Sci U S A* **106**: 4852–4857.
Mauriello, E.M.F., Nan, B., and Zusman, D.R. (2009) AglZ regulates adventurous (A-) motility in Myxococcus xanthus through its interaction with the cytoplasmic receptor, FrzCD. *Mol Microbiol* **72**: 964–977.
Mignot, T., Merlie, J.P., and Zusman, D.R. (2005) Regulated pole-to-pole oscillations of a

bacterial gliding motility protein. *Science* **310**: 855–7.
Moine, A., Agrebi, R., Espinosa, L., Kirby, J.R., Zusman, D.R., Mignot, T., and Mauriello, E.M.F. (2014) Functional organization of a multimodular bacterial chemosensory apparatus. *PLoS Genet* **10**: e1004164.
Parra, M.A., Kerr, D., Fahy, D., Pouchnik, D.J., and Wyrick, J.J. (2006) Deciphering the Roles of the Histone H2B N-Terminal Domain in Genome-Wide Transcription. *Mol Cell Biol* **26**: 3842–3852.
Piñas, G.E., Frank, V., Vaknin, A., and Parkinson, J.S. (2016) The source of high signal cooperativity in bacterial chemosensory arrays. *Proc Natl Acad Sci U S A* **113**: 3335–3340.
Ringgaard, S., Schirner, K., Davis, B.M., and Waldor, M.K. (2011) A family of ParA-like ATPases promotes cell pole maturation by facilitating polar localization of chemotaxis proteins. *Genes Dev* **25**: 1544–1555.
Ringgaard, S., Zepeda-Rivera, M., Wu, X., Schirner, K., Davis, B.M., and Waldor, M.K. (2014) ParP prevents dissociation of CheA from chemotactic signaling arrays and tethers them to a polar anchor. *Proc Natl Acad Sci U S A* **111**: E255-264.
Schindelin, J., Arganda-Carreras, I., Frise, E., Kaynig, V., Longair, M., Pietzsch, T., *et al.* (2012) Fiji: an open-source platform for biological-image analysis. *Nat Methods* **9**: 676–682.
Sievers, F., and Higgins, D.G. (2002) Clustal Omega. In *Current Protocols in Bioinformatics*. John Wiley & Sons, Inc., http://onlinelibrary.wiley.com.gate1.inist.fr/doi/10.1002/0471250953.bi0313s48/abstract. Accessed August 17, 2015.
Sourjik, V., and Berg, H.C. (2000) Localization of components of the chemotaxis machinery of Escherichia coli using fluorescent protein fusions. *Mol Microbiol* **37**: 740–751.
Sourjik, V., and Berg, H.C. (2002) Binding of the Escherichia coli response regulator CheY to its target measured in vivo by fluorescence resonance energy transfer. *Proc Natl Acad Sci U S A* **99**: 12669–12674.
Sourjik, V., and Berg, H.C. (2004) Functional interactions between receptors in bacterial chemotaxis. *Nature* **428**: 437–441.
Strahl, H., Ronneau, S., González, B.S., Klutsch, D., Schaffner-Barbero, C., and Hamoen, L.W. (2015) Transmembrane protein sorting driven by membrane curvature. *Nat Commun* **6**: 8728.
Studdert, C.A., and Parkinson, J.S. (2005) Insights into the organization and dynamics of bacterial chemoreceptor clusters through in vivo crosslinking studies. *Proc Natl Acad Sci U S A* **102**: 15623–15628.
Thiem, S., and Sourjik, V. (2008) Stochastic assembly of chemoreceptor clusters in Escherichia coli. *Mol Microbiol* **68**: 1228–1236.
Thompson, S.R., Wadhams, G.H., and Armitage, J.P. (2006) The positioning of cytoplasmic protein clusters in bacteria. *Proc Natl Acad Sci U S A* **103**: 8209–8214.
Typas, A., and Sourjik, V. (2015) Bacterial protein networks: properties and functions. *Nat Rev Microbiol* **13**: 559–572.

Figure legends

Figure 1. FrzCD-GFP colocalizes with the nucleoid in *M. xanthus*. (A) Micrographs of *M. xanthus* cells carrying a GFP or a mCherry fusion and stained with the DNA DAPI stain. The genetic backgrounds of the *M. xanthus* strains are indicated on the left. The white arrows indicate the cells whose fluorescence profiles and correlation coefficients between the DAPI and GFP localization are shown in (B) and (C), respectively. Cells surrounded by white boxes are taken from separate original micrographs. Scale bars correspond to 1µm. **(B)** GFP or mCherry (green or red) and DAPI fluorescence (blue) profiles with the fluorescence intensity (arbitrary units) represented on the *y* axis and the cell length positions with -1 and +1 indicating the poles, on the *x* axis. **(C)** Correlation coefficients between the DAPI and GFP or mCherry localization. R^2 values > 0,5 indicate significant correlations. **(D)** Box plots indicate the medians of the correlation coefficients (R^2) from 10 cells (from one biological replicate) of each of the indicated strains. **(E)** Micrographs of a *M. xanthus parB* conditional mutant carrying *frzCD-gfp* or *frzE-mCherry* and DAPI stained. Micrographs were obtained upon 18h depletion of ParB. The genetic backgrounds of the *M. xanthus* strains are indicated on the left. Scale bars correspond to 1µm.

Figure 2. FrzCD-GFP colocalizes with the nucleoid in *E. coli*. (A) Micrographs of *E.coli* cells carrying a GFP fusion on a plasmid and stained with the DNA DAPI stain. The genetic fusions are indicated on the left. Cells carrying *frzCD-gfp* were also treated with 10µg/ml cephalexin to visualize FrzCD-GFP colocalization with the multiple nucleoids of undivided cells. The white arrows indicate the cells whose fluorescence profiles are shown in (B). Cells surrounded by white boxes are taken from separate original micrographs. Scale bars correspond to 1µm. **(B)** GFP (green) and DAPI fluorescence (blue) profiles with the fluorescence intensity (arbitrary units) represented on the *y* axis and the cell length positions with -1 and +1 indicating the poles, on the *x* axis. **(C)** Correlation coefficients between the

DAPI and GFP localization. R^2 values > 0,5 indicate significant correlations. **(D)** Box plots indicate the medians of the correlation coefficients (R^2) from 10 cells (from one biological replicate) of each of the indicated strains.

Figure 3. FrzCD directly interacts with the DNA *in vitro*. (A) Electrophoretic mobility shift assays (EMSA) on 1% agarose gels stained with ethidium bromide and developed at the UV light. The indicated concentrations of purified 6His-FrzCD were incubated with a 801 bp DNA fragment. **(B)** Schematic representation of the FrzCD protein domains. **(C-D)** The indicated increasing concentrations of 6His-FrzCD$^{\Delta 131-417}$ (C) and 6His- FrzCD$^{\Delta 1-130}$ (D) were used in EMSA assays with a 801 bp DNA fragment. **(E)** Average binding curves and duplicates in degraded colors of each immobilized FrzCD construct 6His- FrzCD, 6His-FrzCD$^{\Delta 131-417}$ or 6His- FrzCD$^{\Delta 7-27}$, with a 474 bp DNA fragment at a concentration of 38nM**.** **(F)** "Sliding window" representation indicating the protein charge of the first FrzCD N-terminal region at the different positions and obtained with 10, 20 and 30 residue windows (blu, green and red, respectively). **(G)** Increasing concentrations of 6His-FrzCD$^{\Delta 7-27}$ were used in EMSA assays. On the first lane of each gel, 500 ng of the 2-Log DNA ladder (0.1-10 kb, NEB) have been loaded. Data in panel (A, C, D, and G) are representative of three independent experiments.

Figure 4. The organization of FrzCD clusters depends on cluster intensity and mobility. (A) A representative fluorescence 1 second time-lapse (left panel) and the corresponding kymograph (middle panel) of a *frzCD-gfp* cell (top panel). Big and small arrows indicate large and small clusters, respectively. The right panel represents the trajectories of each cluster (same color codes as on the top panel). Scale bars correspond to 1µm. **(B)** Cluster displacement (r) from the mean position at each given time (t). L represents the cell length.

The color code corresponding to the logarithm of the ratio r/L indicates that the amplitude of the cluster displacement never exceeds 5% of the cell length. **(C)** Box plots indicate the distribution of the Mean Square Displacements at the different lag times; the mean of each lag value is indicate by the black dots. **(D)** Box plots indicate a significant decrease of the median confinement for clusters of low fluorescence intensity compared to high intensity clusters. For panels B, C and D 1039 clusters from 297 cells (two biological replicates) were analyzed. **(E)** The box plots and the violin plots show the measured confinements of *frzCD-gfp* strains blocked in the ON ($frzCD_{E168A-G169A}$::*gfp*) and OFF ($frzCD_{E202A-E203A}$::*gfp*) states. 130 and 150 clusters were analyzed for the ON and OFF states, respectively.

Figure 5. Frz cluster formation generates signal sensitivity in turn important for social behaviors. (A) The average reversal frequencies, calculated by scoring FrzS-YFP pole-to-pole oscillations are shown as a function of the IAA concentration for wild type (black), $frzCD^{\Delta 6\text{-}130}$ (red) and *ΔfrzCD* (grey). Reversal frequencies values of wild type and $frzCD^{\Delta 6\text{-}130}$ can be fitted by the Hill equation with an interval of confidence of 95% (dashed lines). Error bars represent the standard errors of the means. Reversal frequency values for each IAA dose and each strain are the results of two independent biological triplicates. About one hundred cells for the wild type and $frzCD^{\Delta 1\text{-}130}$ strains and fifty for the *ΔfrzCD* strain were analyzed (refer to Supplementary Table 3 for the exact number of analyzed cells for each strain and IAA doses used in this experiment). **(B)** Colony expansion of wild type, $frzCD^{\Delta 6\text{-}130}$ and *ΔfrzCD* cells. Error bars represent the standard deviations of the means from three biological replicates. **(C)** The same strains were analyzed in *E. coli* predation assays.

Figure supplements

Figure 1-figure supplement 1. Representative micrographs of *M. xanthus* cells carrying a GFP or a mCherry fusion and stained with the DNA DAPI stain. The genetic backgrounds of the *M. xanthus* strains are indicated on the left. Scale bars correspond to 1μm.

Figure 1-figure supplement 2. *frzE-mCherry* cells can swarm and form fruiting bodies like wild type. Scale bars correspond to 0,5 cm.

Figure 1-figure supplement 3. FrzCD and FrzE are stable in different *M. xanthus* mutants. Western blot with anti-FrzCD **(A)** or anti-FrzE antibodies **(B)** on the cell extracts of the indicated *M. xanthus* strains. Scale bars correspond to 1μm. Black lines are used to indicate that two lanes from the same gel where separated by other lanes there were lanes between separate lanes from different westerns blots.

Figure 1-figure supplement 4. Positive correlation between the number of FrzCD clusters and the nucleoid length (pixels). Average numbers of clusters with standard deviations (black dots and bars, respectively) for different nucleoid sizes are shown. Green dots represent measurements for individual cells. Grey zones represent the variances. 2564 clusters from two biological replicates were analyzed.

Figure 1-figure supplement 5. FrzCD segregated in cells with segregated chromosomes. **(A)** 909 cells were ordered according to their cell length (pixels, grey) and for each cells GFP and DAPI fluorescence are represented as green and blue dots, respectively, at their corresponding cell position. 0 is the cell center. **(B)** The three histograms show the average

GFP (green) and DAPI (blue) fluorescence density for each cell position for the indicated cell-size ranges. 0 is the cell center.

Figure 3-figure supplement 1. FrzCD binds DNA fragments of different lengths, forms a dimer and promotes FrzE phosphorylation. (A- D) Electrophoretic mobility shift assay (EMSA) on agarose gel stained with ethidium bromide and developed at the UV light. DNA fragments of different lengths and GC contents (Table S4) were incubated with increasing concentrations of FrzCD-(His_6) as indicated, including **(A)** 4 nM of Oligo1300 (1% agarose gel), **(B)** 40 nM of Oligo340-1 (38% GC content; 1.5% agarose gel), **(C)** 40 nM of Oligo340-2 (61% GC content; 1.5% agarose gel), and **(D)** 300 nM of Oligo70 (2.5% agarose gel). **(E)** SEC-MALS analysis showing the elution profile (refractive index; black; left y-axis) and the estimated molar masses (green; right y-axis) of the FrzCD eluted protein. **(F)** SDS page of the indicated proteins purified from *E. coli* and used for the different experiments shown in Figure 3. **(G)** Kinetics of the FrzE kinase domain ($FrzE^{CheA}$) auto-phosphorylation were tested *in vitro* by incubation of $FrzE^{CheA}$ in the presence of FrzA , the indicated different form of FrzCD and ATPγP^{33} as a phosphate donor.

Figure 3-figure supplement 2. FrzCD-GFP binds the nucleoid in a DNA-sequence independent manner. A library of DNA fragments was obtained by ChIP experiments on *frzCD-gfp* and *parB-yfp* strains, using GFP polyclonal antibodies. The figure shows the results obtained by the deep sequencing of the DNA libraries. Only for *parB-yfp*, we observed an enrichment corresponding a to the nucleoid region containing *parS* (rectangle in the middle panel and last panel) (Harms *et al.*, 2013) (9,109 to 9,110 Kb). Note that while the number of reads relative to ParB are represented with a logarithmic scale, for FrzCD we used a regular scale.

Figure 3-figure supplement 3. The FrzCD N-terminal tail has the same properties of that of eukaryotic histones. (A) Prediction of the FrzCD N-terminal secondary structures. The nature of each amino acid is also indicated through color codes. **(B)** FrzCD first 50 amino acid alignment with the N-terminal tail of Histones 2B. The alignment was obtained by Clustal Omega. Dots indicate similarities and stars identities.

Figure 3-figure supplement 4. The FrzCD N-terminus from different species show similar amounts of positively charged amino acids. The alignment of FrzCD sequences from the indicated species was obtained by Clustal Omega. Stars indicate identities.

Table S1: Strains used in this study

Strains	Genotyp	Deletion	Source
DZ2	*wt*		Zusman et al., 1982
DZ4620	*frzCD-gfp*		Mauriello et al., 2009
DZ4480	Δ*frzCD*	Codons 6-393	Bustamante et al., 2004
DZ4485	$frzCD^{\Delta 6\text{-}130}$		Mauriello et al., 2009
DZ4743	$frzCD^{\Delta 6\text{-}130}$*-gfp*		Mauriello et al., 2009
EM231	$frzCD_{E202A\text{-}E203A}$*::gfp*		Mauriello et al., 2009
EM228	$frzCD_{E168A\text{-}G169A}$*::gfp*		Mauriello et al., 2009
EM434	*frzE-mCherry*		This study
EM506	*frzE-mCherry* Δ*frzCD*		This study
EM516	*frzCD-gfp frzE::kan*	Codons 171-438	This study
EM531	*difA-gfp* Δ*parB*/P_{cuoA}*-parB*		This study
EM532	*frzCD-gfp* Δ*parB*/P_{cuoA}*-parB*		This study
EM533	*frzE-mCherry* Δ*parB*/P_{cuoA}*-parB*		This study
EM543	$frzCD^{\Delta 7\text{-}27}$	Codons 7-27	This study
EM550	$frzCD^{\Delta 7\text{-}27}$*-gfp*	Codons 7-27	This study
TM26	*frzS-yfp*		Guzzo et al., 2015
EM622	$frzCD^{\Delta 6\text{-}130}$ *frzS-yfp*		This study
EM623	Δ*frzCD frzS-yfp*		This study

Table S2: Plasmids used in this study

Plasmid	Expression plasmid	Source
pAH57	P_{cuoA}*-parB,* copper-dependent expression of *parB*, Mx8 attB	Harms et al., 2013
pAH18	Construct for in frame deletion of *parB*	Harms et al., 2013
pETPhos_*frzCD*	pETPhos with *frzCD* tagged with 6-his inducible with IPTG	Guzzo et al., 2015
pETPhos_$frzE^{kinase}$	pETPhos with $frzE^{CheA}$ tagged with 6-his inducible with IPTG	Guzzo et al., 2015
pETPhos_$frzCD^{c}$	pETPhos with $frzCD^{c}$ tagged with 6-his inducible with IPTG	Guzzo et al., 2015
pGEX(M)_*frzA*	pETPhos with *frzA* tagged with 6-his inducible with IPTG	Guzzo et al., 2015
pEM365	pBJ113 with frzE-mCherry fusion	This study
pEM405	pBJ113 with an insertion cassette for *frzE::kan*	This study
pEM418	pBJ113 with a cassette for $frzCD^{\Delta 7\text{-}27}$	This study
pEM414	pETPhos with $frzCD^{\Delta 1\text{-}130}$ tagged with 6-his inducible with IPTG	This study
pEM415	pETPhos with $frzCD^{\Delta 131\text{-}417}$ tagged with 6-his inducible with IPTG	This study
pEM433	pETPhos with $frzCD^{\Delta 7\text{-}27}$ tagged with 6-his inducible with IPTG	This study
pEM409	pETDuet-1 with *frzCD-gfp* inducible with IPTG	This study
pEM417	pETDuet-1 with $frzCD^{\Delta 1\text{-}130}$*-gfp* inducible with IPTG	This study
pEM434	pETDuet-1 with $frzCD^{\Delta 7\text{-}27}$*-gfp* inducible with IPTG	This study
pEFrzSY	pEYFPN1 with a cassette to construct *frzS-yfp*	Guzzo et al., 2015
pFCD-H6	pHis17 with *frzCD* gene tagged with a C-terminal 6-his	This study

Table S3: Number of cells analyzed for Figure 5A

Strain \ %IAA	**0**	**0.005**	**0.01**	**0.03**	**0.05**	**0.1**	**0.3**
frzS-yfp	101	113	77	114	64	47	170
frzCD*$^{\Delta 6\text{-}130}$ *frzS-yfp	98	103	75	128	112	139	109
Δ*frzCD frzS-yfp*	44	ND	ND	ND	48	ND	47

Table S4: DNA sequences used for EMSA in Figure 3 and Supplementary figure 4

Ds DNA	Sequence (5' → 3')	Length, GC content (%)
Oligo70	CTTGCAGTAGAGCTGACCATGATTACGCCATCAGCAGCTCCAGGTCGTAC CTCCAGCTACCAATCCCCG	69, 57
Oligo340-1	TAATACGACTCACTATAGGGAGACCACAACGGTTTCCCTCTAGAAATAAT TTTGTTTAACTTTAAGAAGGAGATATACATATGTCCCTGGACACCCCCAA CGAGAAGCCCGCTGGCAAGGCTCGCGCCCGGAAGGCCCCCGCCTCCAAGG CCGGCGCCACGAACGCGGCGTCGACCTCTTCCTCCACCAAGGCCATCACC GACACGCTGCTGACGGTGCTGTCCGGCAACCTGCAGGCCCGCGTGCCCAA GGAGCTGGTCGGTGAGTCCGGCGTGGAGCTGGCGCACCTGCTCAACCAGG TGCTGGACCAGTTCGCGGCCTCCGAGCACCGCAAGCATG	339, 61
Oligo340-2	GTTTAACTTTAAGAAGGAGATATACATATGAAAAAAGAAACGATTTTTTC CGAAGTAGAAACGGCTAACAGCAAGCAACTGGCTGTGTTGAAAGCTAATT TCCCACAGTGTTTTGATAAAAACGGAGCCTTCATTCAAGAAAAATTGCTT GAGATTATTAGGGCATCGGAAGTTGAACTCTCTAAAGAATCATACAGCTT GAACTGGCTGGGTAAATCTTATGCCCGTTTGTTGGCCAATCTACCACCGA AAACGTTGTTGGCAGAAGATAAAACTCATAACCAACAAGAAGAGAACAAG AACAGTCAACACCTGTTAATCAAAGGGGATAATCTCGAAGTATTG	345, 38
Oligo1300	*frzCD* gene amplified with the primers 5'-ATGTCCCTGGACACCCCCAACGAGAAGCCCGCTGG-3'and 5'-CTAGTCGGCCTTGAACCGCTTGATGAGCTCGGCCA-3' and the plasmid pFCD-H6 as template	1254, 70
Oligo801	Fragment amplified with the primers 5'-cgggatcctggctccgcccccgacgca-3' and 5'-cccaagcttttgatgaggcgcttggagat-3' and DZ2 chromosomal DNA as template	801, 68

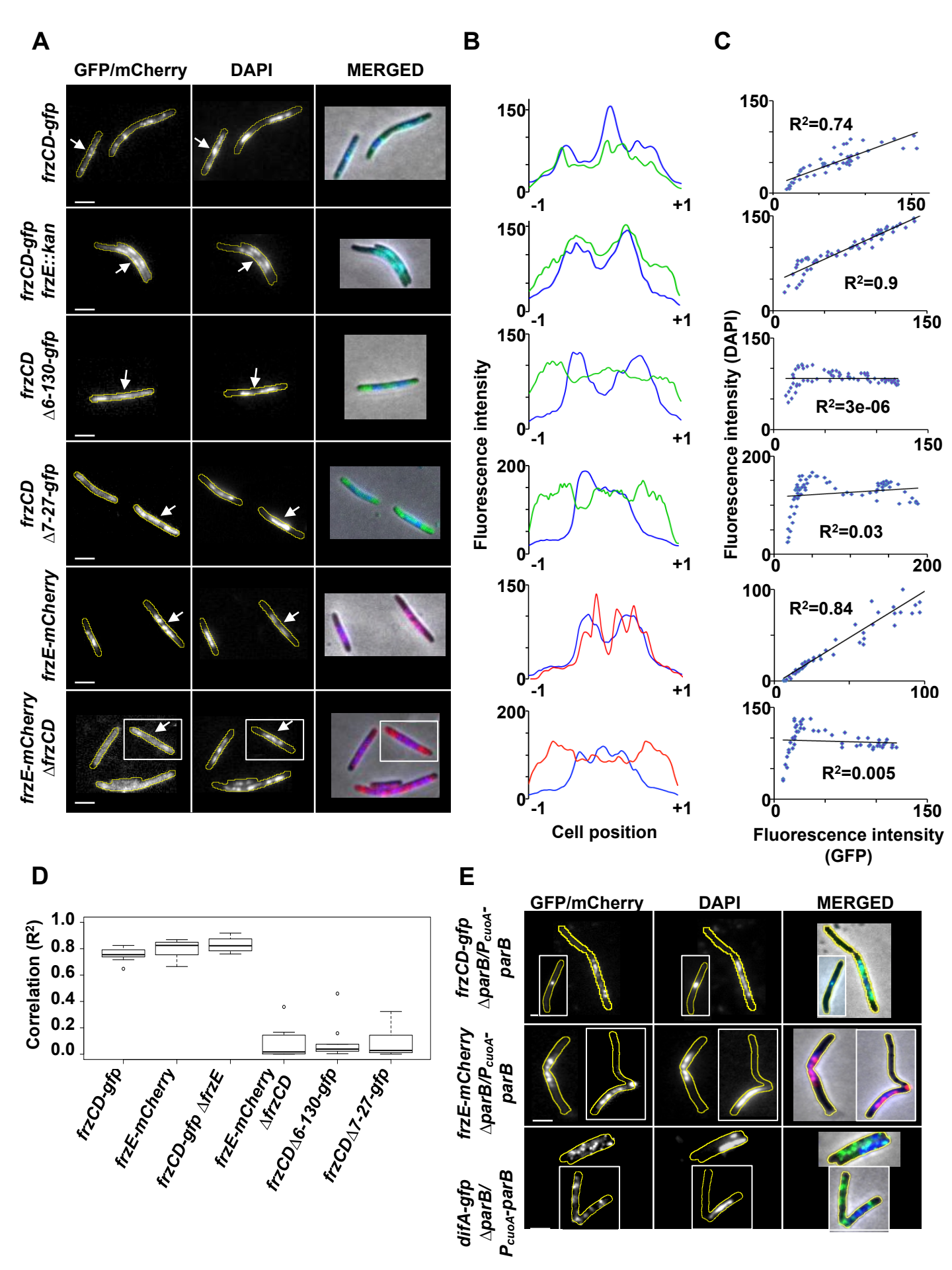
A
GFP/mCherry
DAPI
MERGED
frzCD-gfp
frzCD-gfp frzE::kan
frzCD Δ6-130-gfp
frzCD Δ7-27-gfp
frzE-mCherry
frzE-mCherry ΔfrzCD
B
Fluorescence intensity
Cell position
C
R²=0.74
R²=0.9
R²=3e-06
R²=0.03
R²=0.84
R²=0.005
Fluorescence intensity (DAPI)
Fluorescence intensity (GFP)
D
Correlation (R²)
frzCD-gfp
frzE-mCherry
frzCD-gfp ΔfrzE
frzE-mCherry ΔfrzCD
frzCDΔ6-130-gfp
frzCDΔ7-27-gfp
E
GFP/mCherry
DAPI
MERGED
frzCD-gfp ΔparB/PcuoA-parB
frzE-mCherry ΔparB/PcuoA-parB
difA-gfp ΔparB/ PcuoA-parB

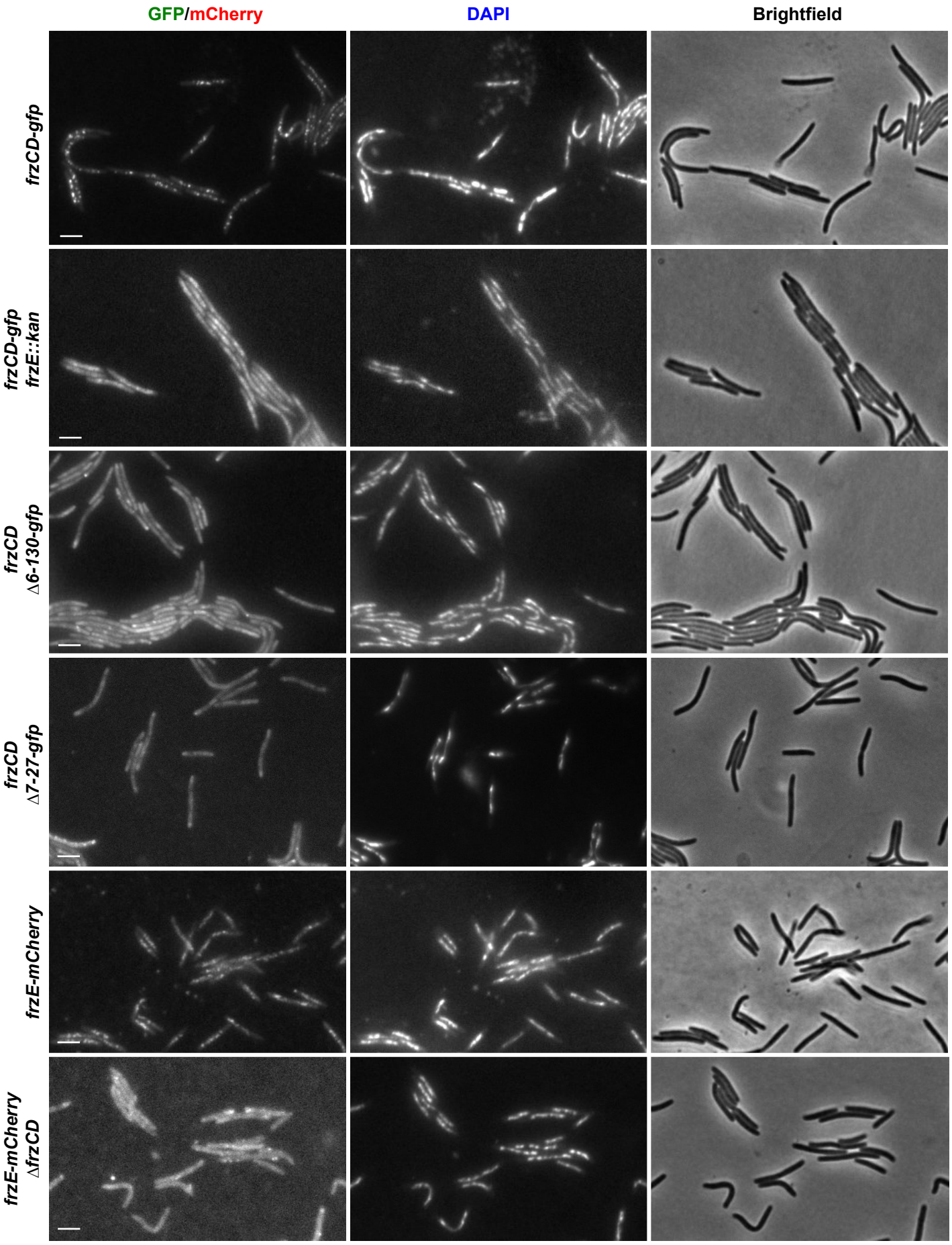
GFP/mCherry
DAPI
Brightfield
frzCD-gfp
frzCD-gfp frzE::kan
frzCD Δ6-130-gfp
frzCD Δ7-27-gfp
frzE-mCherry
frzE-mCherry ΔfrzCD

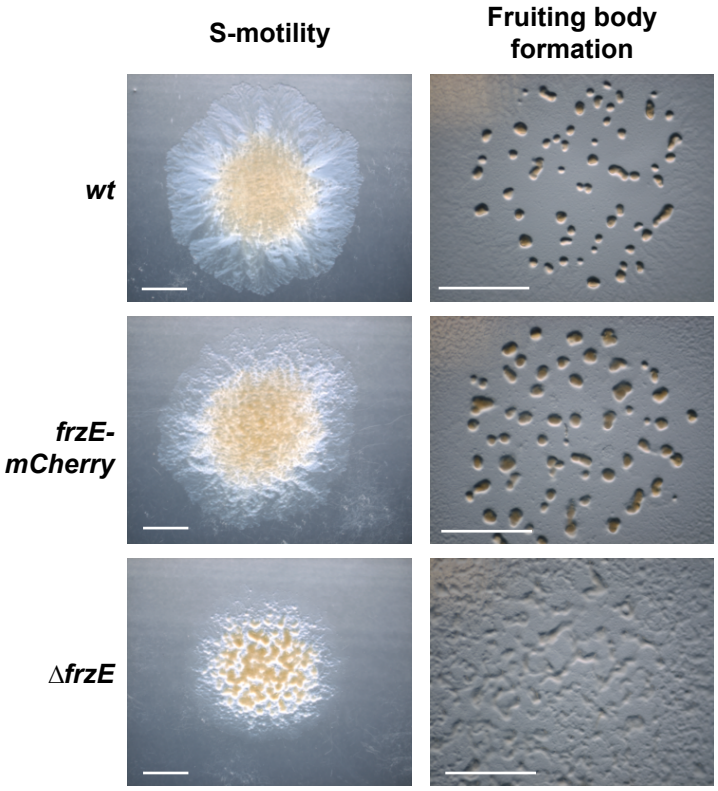
S-motility
Fruiting body formation
wt
frzE-mCherry
ΔfrzE

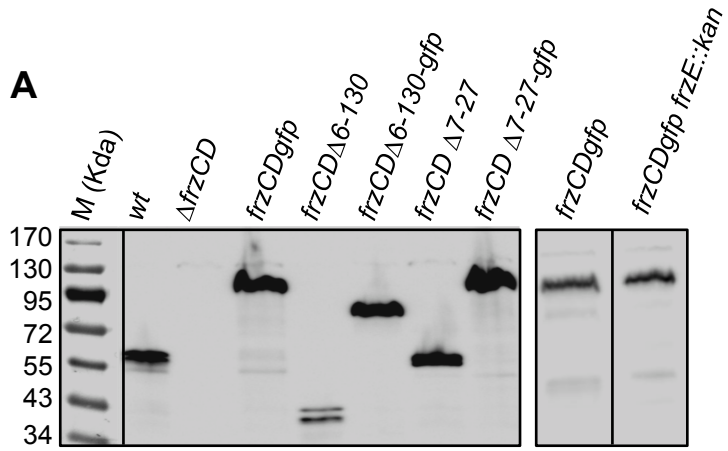
A
M (Kda)
wt
ΔfrzCD
frzCDgfp
frzCDΔ6-130
frzCDΔ6-130-gfp
frzCD Δ7-27
frzCD Δ7-27-gfp
frzCDgfp
frzCDgfp frzE::kan
170
130
95
72
55
43
34

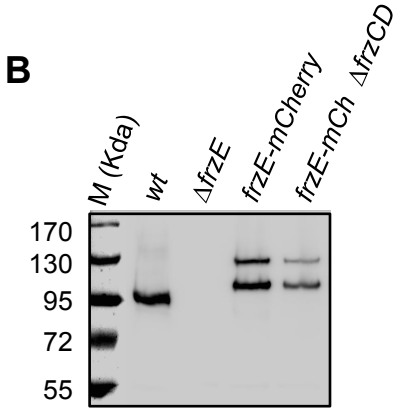
B
M (Kda)
wt
ΔfrzE
frzE-mCherry
frzE-mCh ΔfrzCD
170
130
95
72
55

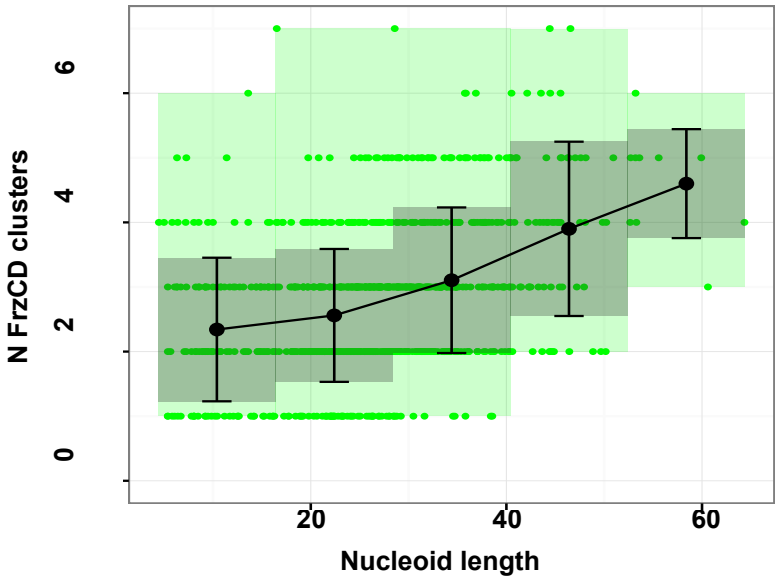
N FrzCD clusters
0
2
4
6
20
40
60
Nucleoid length

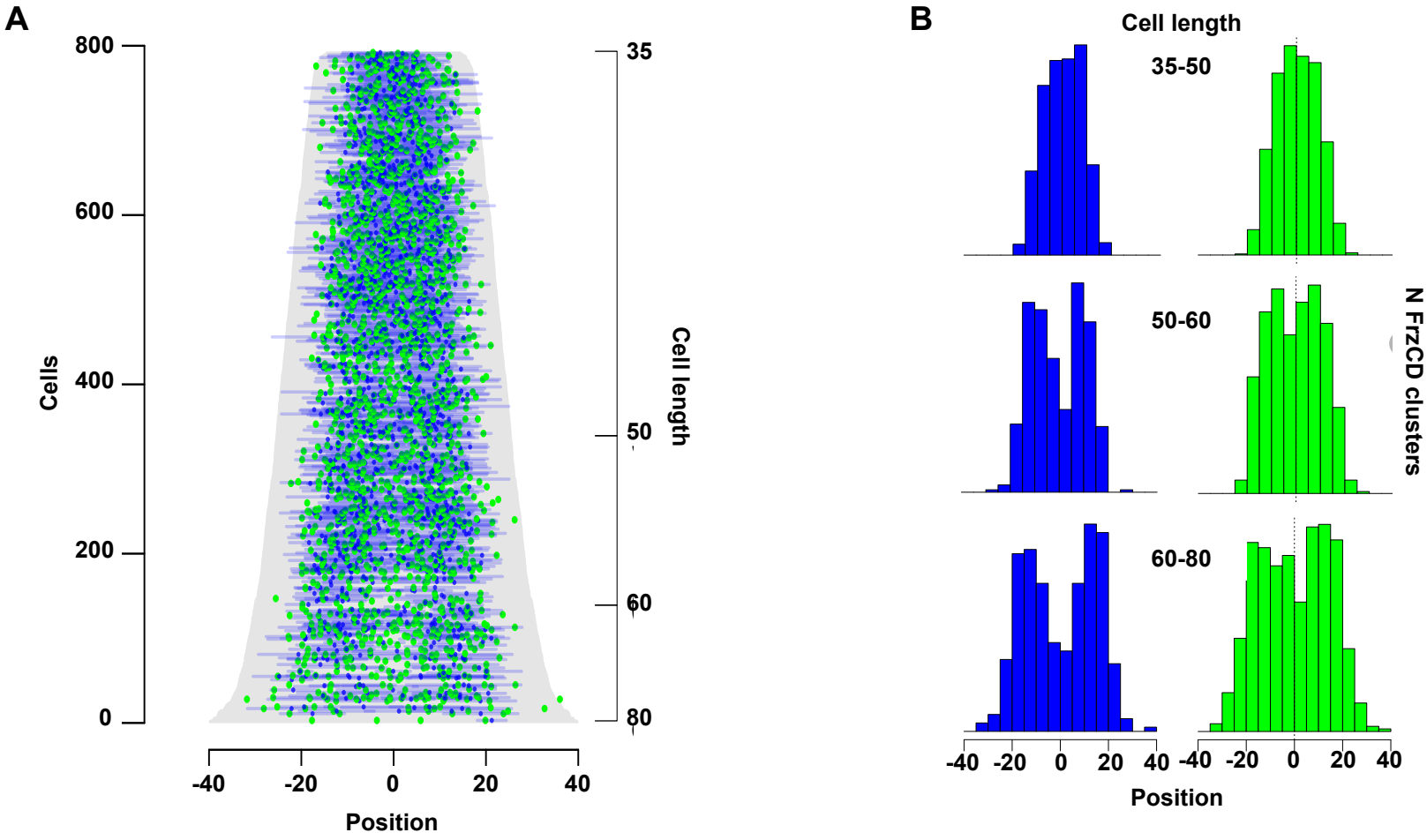
A
800
600
400
200
0
Cells
35
50
60
80
Cell length
-40
-20
0
20
40
Position
B
Cell length
35-50
50-60
60-80
N FrzCD clusters
-40
-20
0
20
40
Position

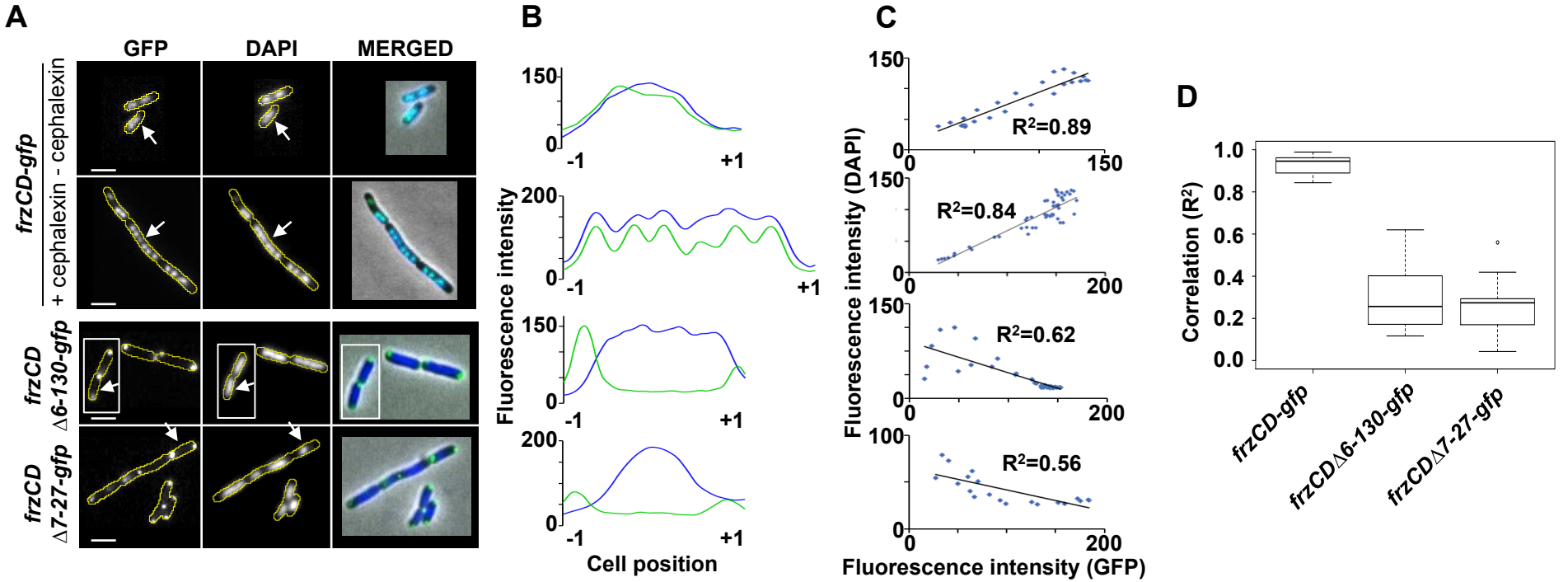
A
GFP
DAPI
MERGED
frzCD-gfp
+ cephalexin - cephalexin
frzCD Δ6-130-gfp
frzCD Δ7-27-gfp
B
Fluorescence intensity
Cell position
C
Fluorescence intensity (DAPI)
Fluorescence intensity (GFP)
R²=0.89
R²=0.84
R²=0.62
R²=0.56
D
Correlation (R²)
frzCD-gfp
frzCDΔ6-130-gfp
frzCDΔ7-27-gfp

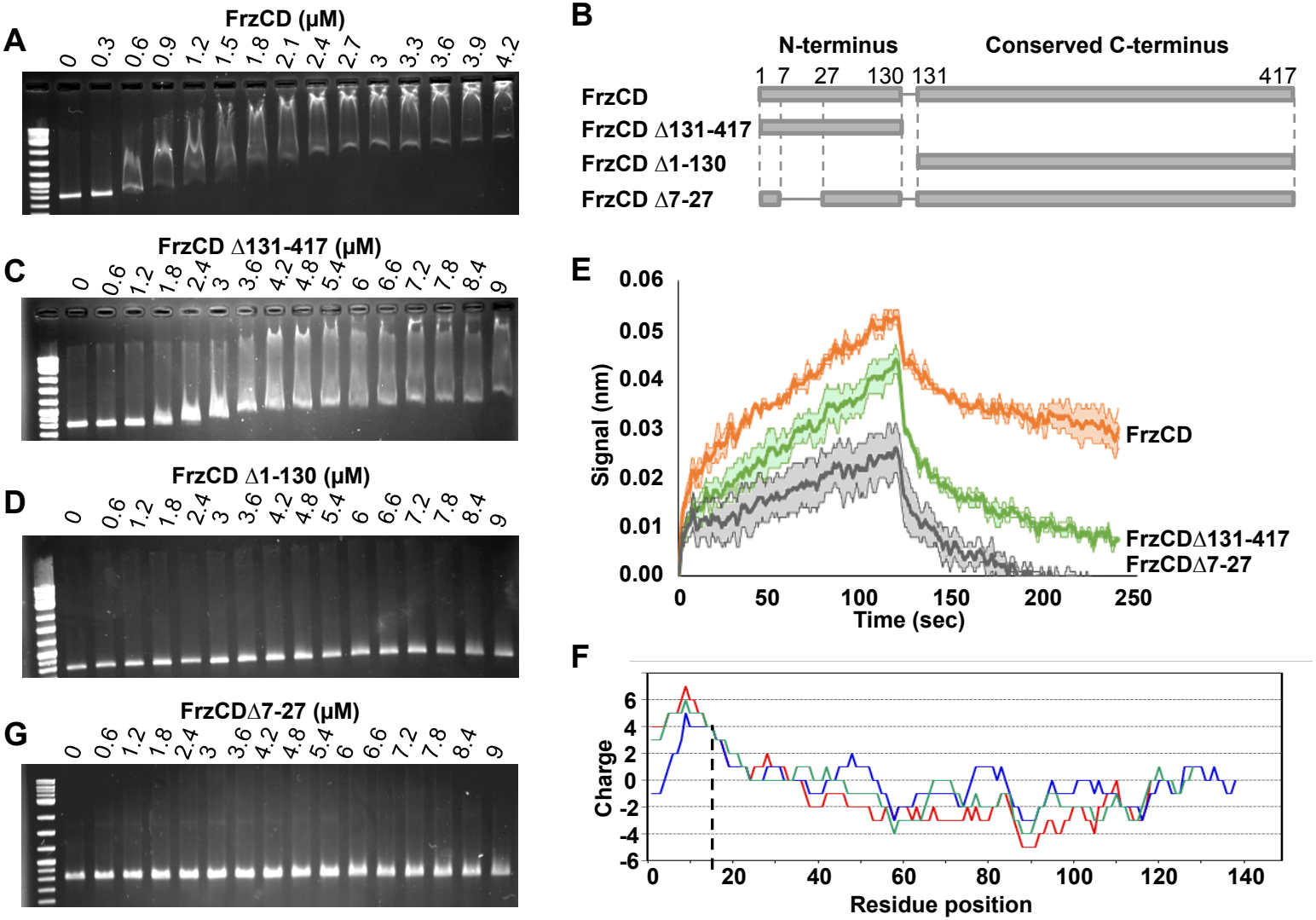
A
FrzCD (μM)
0 0.3 0.6 0.9 1.2 1.5 1.8 2.1 2.4 2.7 3 3.3 3.6 3.9 4.2
B
N-terminus
Conserved C-terminus
1 7 27 130 131 417
FrzCD
FrzCD Δ131-417
FrzCD Δ1-130
FrzCD Δ7-27
C
FrzCD Δ131-417 (μM)
0 0.6 1.2 1.8 2.4 3 3.6 4.2 4.8 5.4 6 6.6 7.2 7.8 8.4 9
D
FrzCD Δ1-130 (μM)
0 0.6 1.2 1.8 2.4 3 3.6 4.2 4.8 5.4 6 6.6 7.2 7.8 8.4 9
E
Signal (nm)
0.06
0.05
0.04
0.03
0.02
0.01
0.00
0 50 100 150 200 250
Time (sec)
FrzCD
FrzCDΔ131-417
FrzCDΔ7-27
F
Charge
6 4 2 0 -2 -4 -6
0 20 40 60 80 100 120 140
Residue position
G
FrzCDΔ7-27 (μM)
0 0.6 1.2 1.8 2.4 3 3.6 4.2 4.8 5.4 6 6.6 7.2 7.8 8.4 9

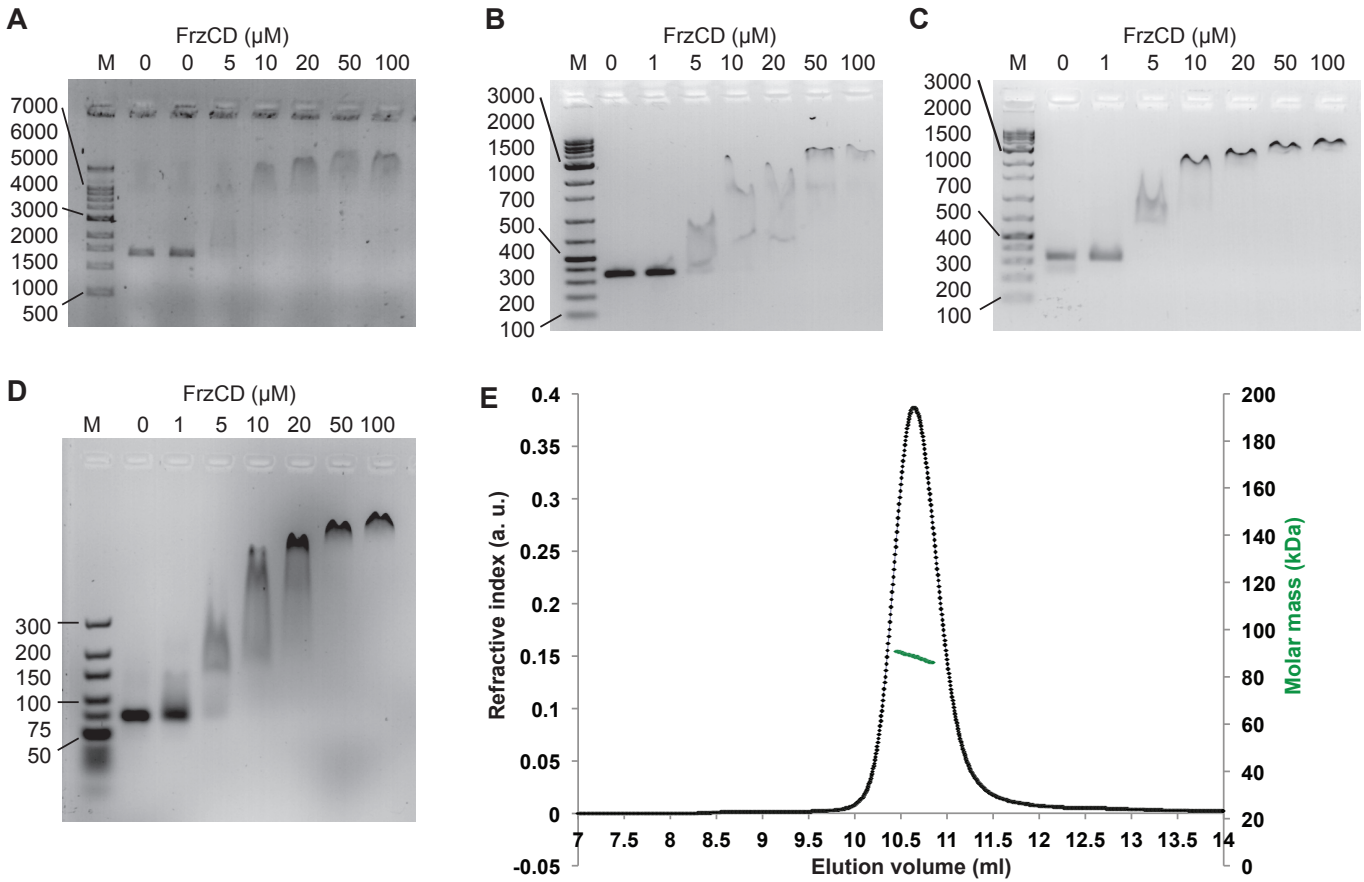
A
FrzCD (μM)
M 0 0 5 10 20 50 100
7000
6000
5000
4000
3000
2000
1500
1000
500
B
FrzCD (μM)
M 0 1 5 10 20 50 100
3000
2000
1500
1000
700
500
400
300
200
100
C
FrzCD (μM)
M 0 1 5 10 20 50 100
3000
2000
1500
1000
700
500
400
300
200
100
D
FrzCD (μM)
M 0 1 5 10 20 50 100
300
200
150
100
75
50
E
Refractive index (a. u.)
0.4
0.35
0.3
0.25
0.2
0.15
0.1
0.05
0
-0.05
7 7.5 8 8.5 9 9.5 10 10.5 11 11.5 12 12.5 13 13.5 14
Elution volume (ml)
Molar mass (kDa)
200
180
160
140
120
100
80
60
40
20
0
F
M (Kda)
FrzCD
FrzCDΔ1-130
FrzCDΔ7-27
FrzCDΔ131-417
M (Kda)
72
55
43
34
26
17
G
M (kDa)
FrzCD_WT
FrzCDc
FrzCDΔ6-130
FrzCDΔ131-417
FrzCDΔ7-27
-
95
72
FrzE_kinase

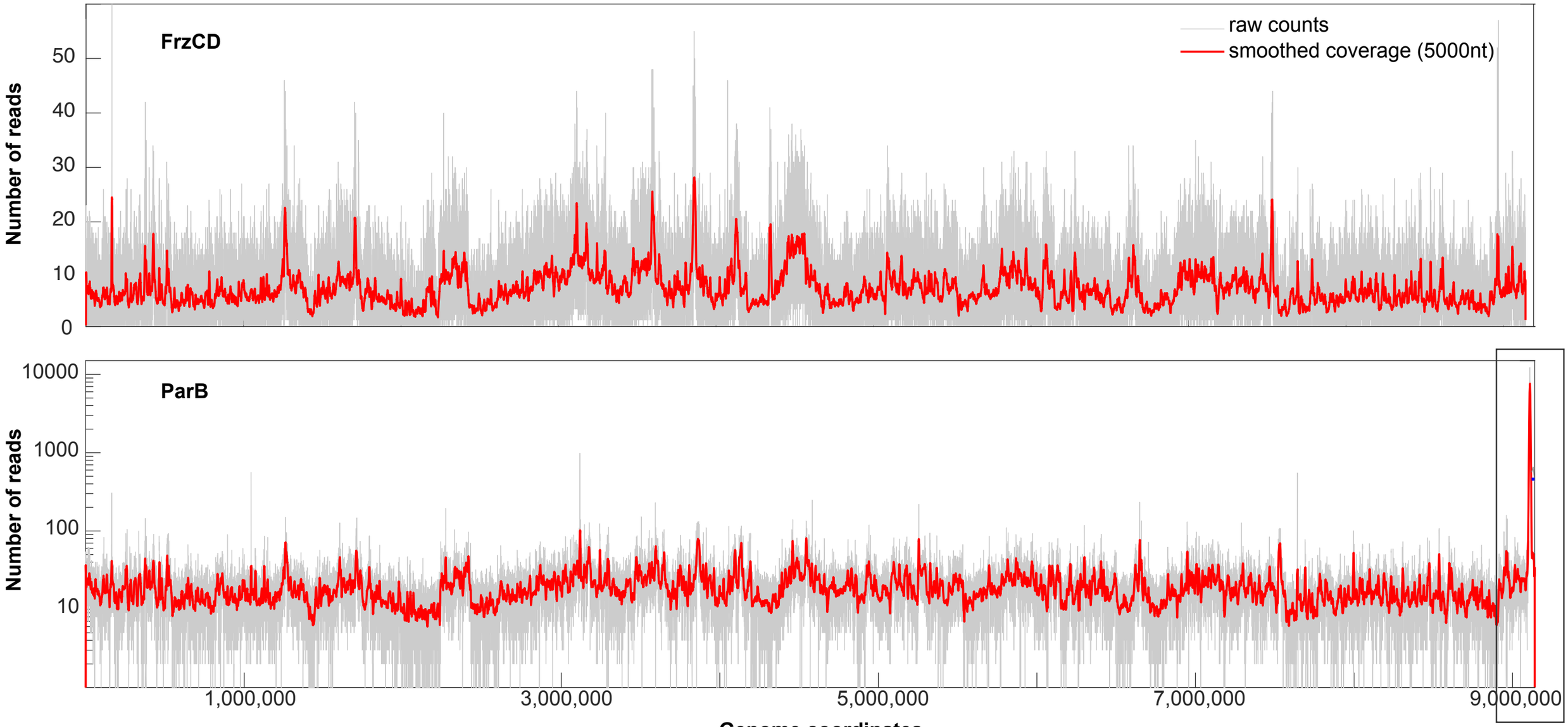
FrzCD
raw counts
smoothed coverage (5000nt)
Number of reads
0
10
20
30
40
50

ParB
Number of reads
10
100
1000
10000
1,000,000
3,000,000
5,000,000
7,000,000
9,000,000
Genome coordinates

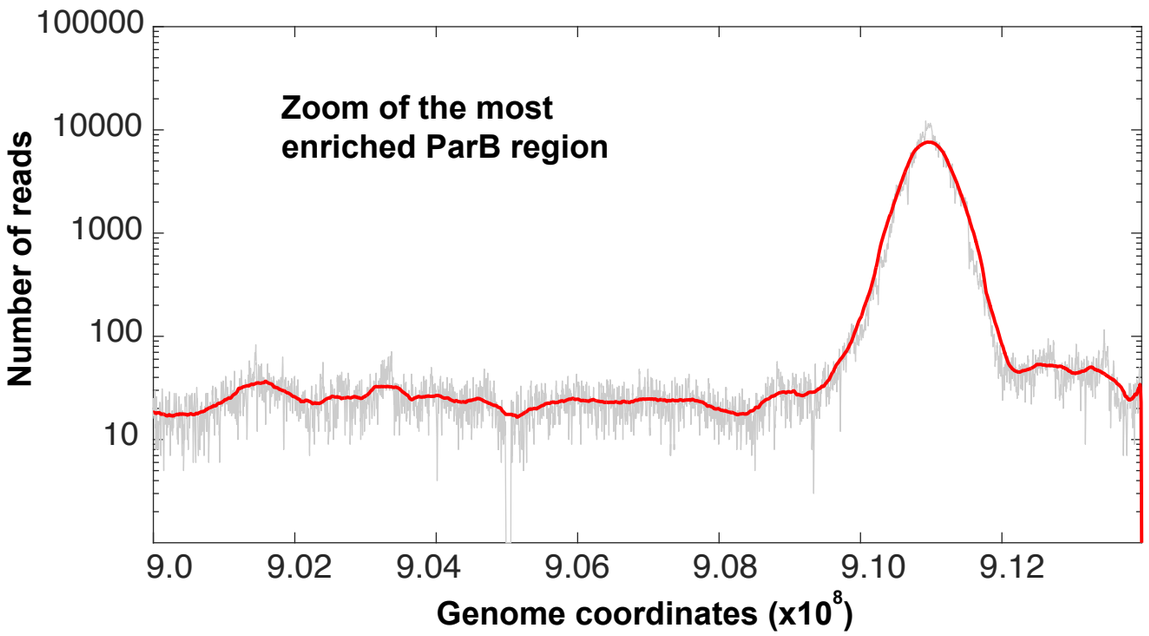
Zoom of the most
enriched ParB region
Number of reads
10
100
1000
10000
100000
9.0
9.02
9.04
9.06
9.08
9.10
9.12
Genome coordinates (x10^8)

```
                 : 1---------11--------21--------31--------41--------51--------61--------71--------81--------91--------101-------111-------121-------131-------141---- :
OrigSeq          : MSLDTPNEKPAGKARARKAPASKAGATNAASTSSSTKAITDTLLTVLSGNLQARVPKELVGESGVELAHLLNQVLDQFAASEHRKHVAAQEIDQALDALIGLVREGDLSRWNTTTEDPQLGPLLEGFGKVIETLRTFVREINEAALR : OrigSeq
Jnet             : ------------HHHH-----HHHHH---------HHHHHHHHHHHH---------------HHHHHHHHHHHHHHHHHHHHHHHHHHHHHHHHHHHHHHHHHHH-----------------HHHHHHHHHHHHHHHHHHHHHHHHH-- : Jnet
jhmm             : ------------HHHH---HHHHHHHH-------HHHHHHHHHHHHH----------HH----HHHHHHHHHHHHHHHHHHHHHHHHHHHHHHHHHHHHHHHHHH-----------------HHHHHHHHHHHHHHHHHHHHHHHHH-- : jhmm
jpssm            : -------------HHHH------------------HHHHHHHHHHH---------------HHHHHHHHHHHHHHHHHHHHHHHHHHHHHHHHHHHHHHHHHHH--------------HHHHHHHHHHHHHHHHHHHHHHHHHHH-- : jpssm
PSIPRED          : ------------HHHHH------------------HHHHHHHHHHHHH--------------HHHHHHHHHHHHHHHHHHHHHHHHHHHHHHHHHHHHHHHHHHH--------------HHHHHHHHHHHHHHHHHHHHHHHHHHHH- :
Phyre2           :------------hHHHHHh-hHHHh---hhhhhhhhhHHHHHHHHHHHH--hhhh--HHHH-----HHHHHHHHHHHHHHHHHHHHHHHHHHHHHHHHHHHHHHHHHH-hhhhh---------hhHHHHHHHHHHHHHHHHHHHHH---- :
```

```
MSLDTPNEKPAGKARARKAPASKAGATNAASTSSSTKAITDTLLTVLSGNLQARVPKELVGESGVELAHLLNQVLDQFAASEHRKHVAAQEIDQALDALIGLVREGDLSRWNTTTEDPQLGPLLEGFGKVIETLRTFVREINEAALR
          |---basic region-----|     loop  |--------------------------------------------------------helical fold--------------------------------------------------------|
                                                                                                                              |____________________________________________
```

RK basic   ED acid   SQN hydrophilic   PATG borderline   LIVMWFY hydrophobic   H histidine

```
frzCD                     MSLDTPNEKPA--------GKARARKAPASKAGATNAAS-TSSSTKAITDTLLTVLSGNL
SP|P04913|H2B1_SCHPO      --MSAAEKKPA--------SKAPAGKAPRDTM-----KSADKKRGKNRKETYSSYIYKVL
SP|A5DJJ1|H2B1_PICGU      -MAPKAEKKPA--------SKAPAEKKPAAKKTA-ST--DSKKRTKTRKETYSSYIYKVL
SP|A5DBG5|H2B2_PICGU      -MAPKAEKKPA--------SKAPAEKKPAAKKTA-SS--DSKKRTKTRKETYSSYIYKVL
SP|Q6BKW7|H2B2_DEBHA      -MAPKAEKKPA--------SKAPAEKKPAAKKTA--T-SGTKKRSKTRKETYSSYIYKVL
SP|Q6BRG2|H2B1_DEBHA      -MAPKAEKKPA--------SKAPAEKKPAAKKTA-SA-TGTKKRSKTRKETYSSYIYKVL
SP|A3LZZ1|HSB1_PICST      MAPPKAEKKPA--------SKAPAEKKPAAKKTA-SATD-SKKRTKTRKETYSSYIYKVL
SP|A5DWF0|H2B_LODEL       -MAPKAEKKPA--------SKAPAEKKPAAKKTA-SSTDGGKKRTKARKETYSSYIYKVL
SP|P48989|H2B1_CANAL      -MAPKAEKKPA--------SKAPAEKKPAAKKTA--STDGAKKRTKARKETYSSYIYKVL
SP|Q59VP1|H2B2_CANAL      -MAPKAEKKPA--------SKAPAEKKPAAKKTA--STDGAKKRTKARKETYSSYIYKVL
SP|Q6FM30|H2B2_CANGA      -MSAKAEKKPA--------SKAPAEKKPAAKKTA-PSSD-GKKRTKARKETYSSYIYKVL
SP|Q6FWM8|H2B1_CANGA      ---MSAEKKPA--------SKAPAEKKPAAKKTA-PSAD-GKKRTKARKETYSSYIYKVL
SP|P02294|H2B2_YEAST      -MSSAAEKKPA--------SKAPAEKKPAAKKTS-TSVD-GKKRSKVRKETYSSYIYKVL
SP|P02293|H2B1_YEAST      -MSAKAEKKPA--------SKAPAEKKPAAKKTS-TSTD-GKKRSKARKETYSSYIYKVL
SP|Q8J1F8|H2B2_ASHGO      -MAPK------A--------EKKPASKAPAAKKTT-ASTDASKKRTKTRKETYSSYIYKVL
SP|Q74ZL5|H2B1_ASHGO      -MSSKASKAPA--------SKAPAEKKPAAKKTS-SSVDASKKRTKTRKETYSSYIYKVL
SP|Q6CK60|H2B1_KLULA      -MSAKASKAPA--------SKAPAEKKPAAKKTS-SSTDPSKKRTKARKETYSSYIYKVL
SP|Q6CMV8|H2B2_KLULA      -MAPKAEKKPA--------SKAPAEKKPAAKKTS-SSVDPSKKRTKARKETYSSYIYKVL
SP|Q6C4I7|H2B_YARLI       MAPKVAEKKPSLAGKAPA-GKAPAEKKEAGKKTT-TATGEKKKRTKARKETYSSYIYKVL
SP|Q0U1A0|H2B_PHANO       MPPK-AQKTPTTGGKAPA-GKAPVEKKEAGKKTA-APSGEKKKRTKTRKETYSSYIYKVL
SP|Q8J1K2|H2B_ROSNE       MPPKAADKKPAAKAP--V-ASKAPEKKDAGKKT--ASTGEKKKRTKARRETYSSYIYKVL
SP|Q4HTT2|H2B_GIBZE       MAPKAADKKPASKAP--ATASKAPEKKDAGKKT--AASGDKKKRSKSRKETYSSYIYKVL
:              *    .          ..  *   :*  : :   *
```

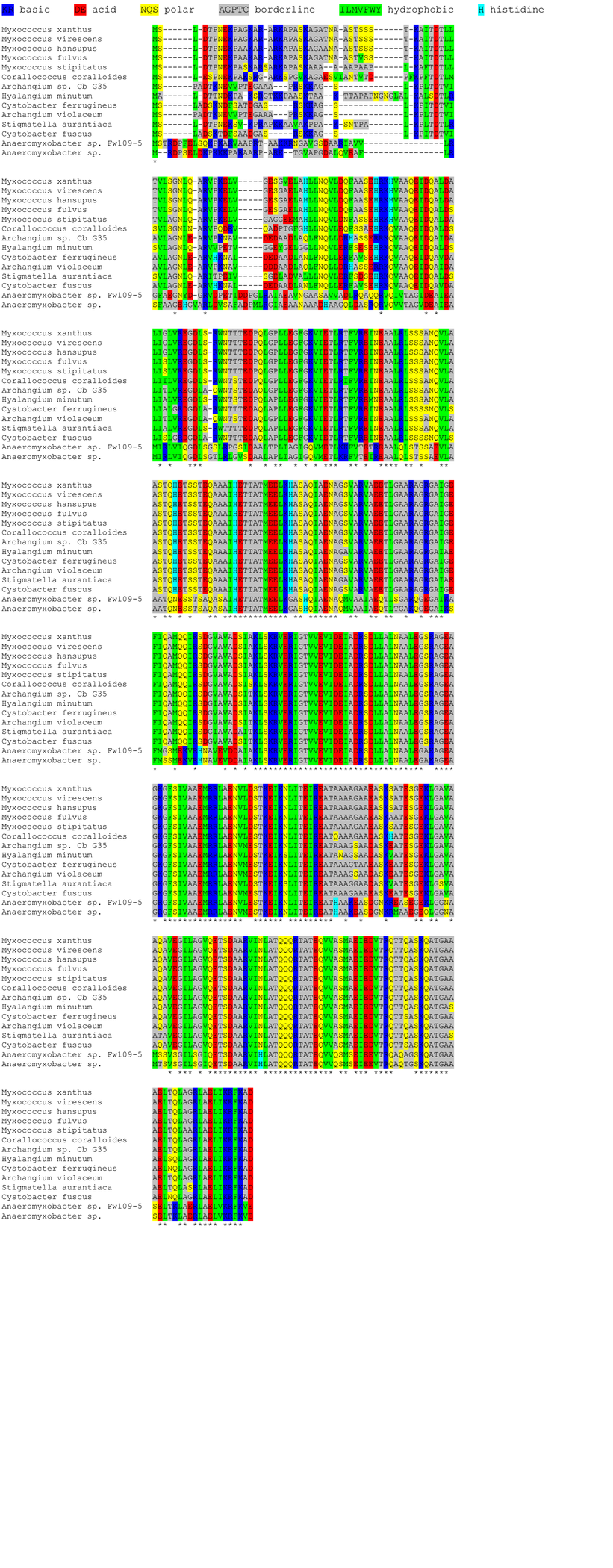
KR basic
DE acid
NQS polar
AGPTC borderline
ILMVFWY hydrophobic
H histidine
Myxococcus xanthus
Myxococcus virescens
Myxococcus hansupus
Myxococcus fulvus
Myxococcus stipitatus
Corallococcus coralloides
Archangium sp. Cb G35
Hyalangium minutum
Cystobacter ferrugineus
Archangium violaceum
Stigmatella aurantiaca
Cystobacter fuscus
Anaeromyxobacter sp. Fw109-5
Anaeromyxobacter sp.

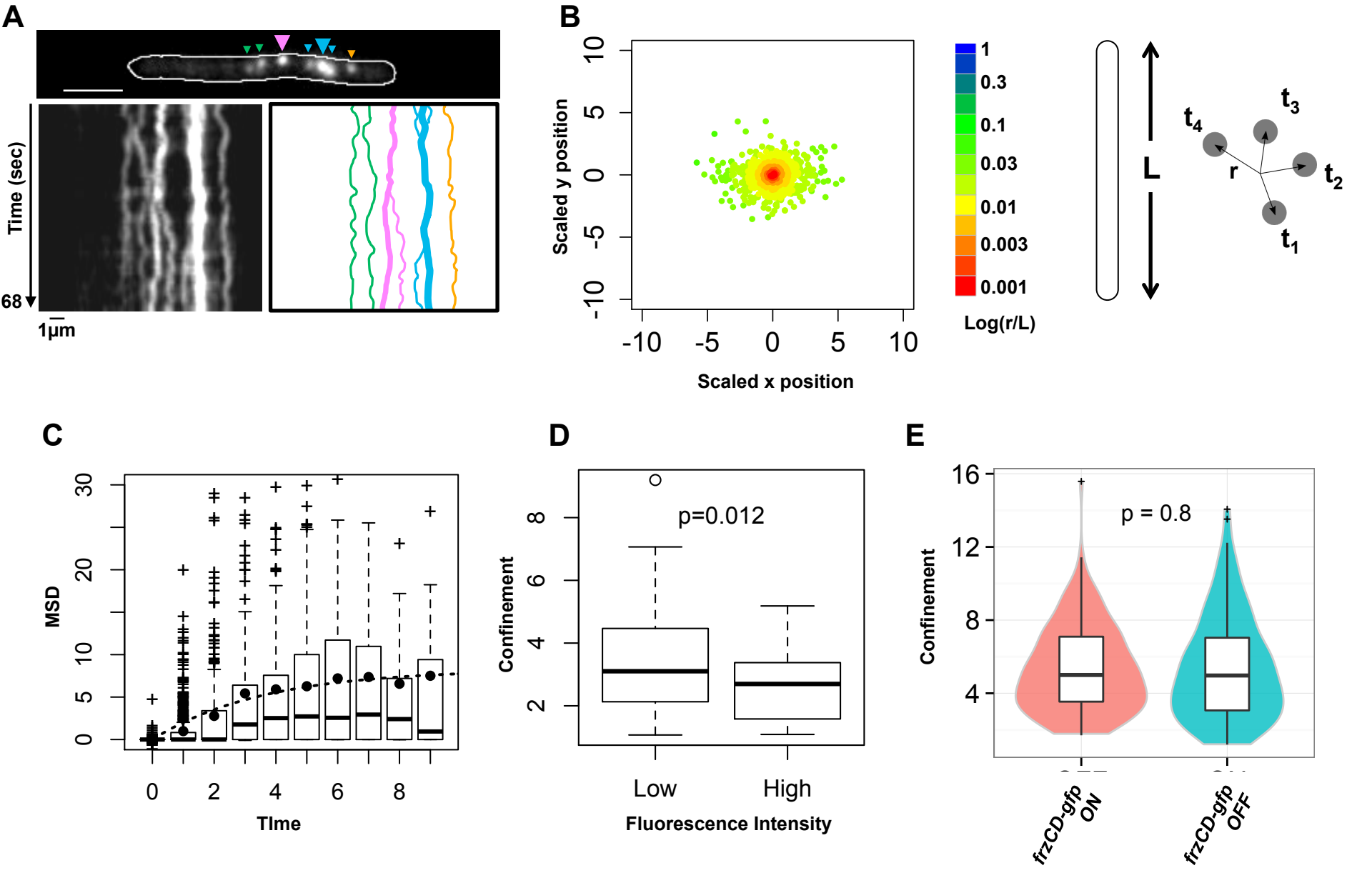
A
Time (sec)
68
1μm
B
Scaled y position
Scaled x position
1
0.3
0.1
0.03
0.01
0.003
0.001
Log(r/L)
L
t3
t4
r
t2
t1
C
MSD
TIme
D
Confinement
p=0.012
Low
High
Fluorescence Intensity
E
Confinement
p = 0.8
frzCD-gfp ON
frzCD-gfp OFF

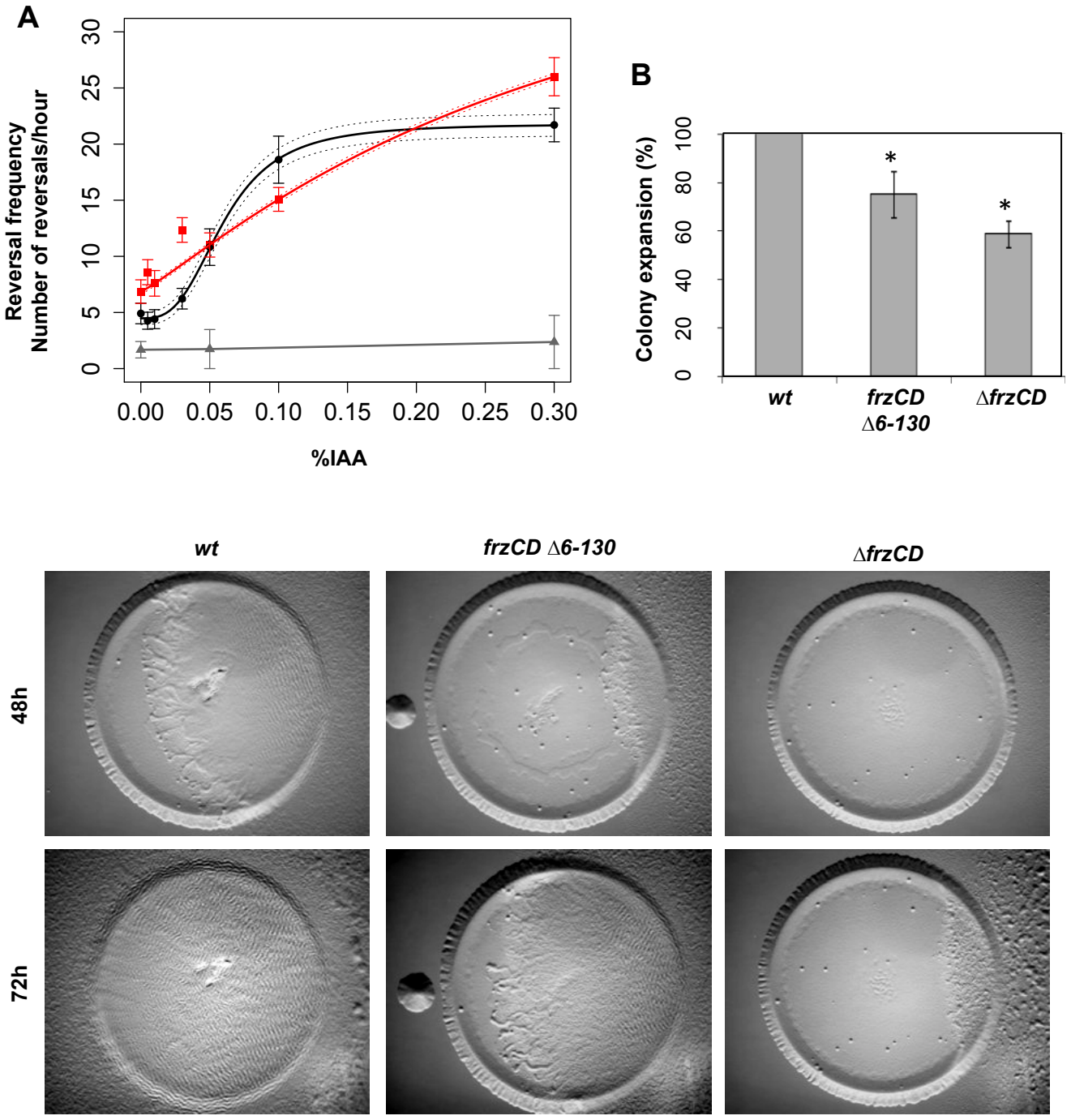
A
Reversal frequency
Number of reversals/hour
0
5
10
15
20
25
30
0.00
0.05
0.10
0.15
0.20
0.25
0.30
%IAA
B
Colony expansion (%)
0
20
40
60
80
100
*
*
wt
frzCD
Δ6-130
ΔfrzCD
C
wt
frzCD Δ6-130
ΔfrzCD
48h
72h